An Integrated Smoothed Particle Hydrodynamics Model for Complex Interfacial Flows with Large Density Ratios

G.X. Zhu[a, b,c], L. Zou[a, b*]

[a] *State Key Laboratory of Structural Analysis for Industrial Equipment, Dalian, 116024, China*

[b] *School of Naval Architecture, Dalian University of Technology, Dalian, 116024, China*

[c] *School of Engineering, University of Plymouth, Drake Circus, Plymouth PL4 8AA, United Kingdom*

Abstract

In this paper, an integrated smoothed particle hydrodynamics (SPH) model for complex interfacial flows with large density ratios is developed. The discrete continuity equation and acceleration equation are obtained by considering the time derivative of the volume of particle and Eckart's continuum Lagrangian equation. A continuum surface force model is used to meet the fact that surface force may not be distributed uniformly on each side of the interface. An improved boundary condition is imposed to model wall free-slip and no-slip condition for interfacial flows with large density ratios. Particle shifting algorithm (PSA) is added for interfacial flows by imposing the normal correction near the interface, called as Interface-PSA. Then four representative numerical examples, including droplet deformation, Rayleigh-Taylor instability, dam breaking, and bubble rising, are presented and compare well with reference data. It is demonstrated that inherent interfacial flow physics can be well captured, including surface tension and the dynamic evolution of the complex interfaces.

Keywords: Smoothed Particle Hydrodynamics; Interfacial Flow; Surface Tension; Particle Shifting.

* Corresponding author. Tel.: +86-0411-84706373

E-mail address: lizou@dlut.edu.cn (L. Zou)

This article has been accepted for publication and undergone full peer review but has not been through the copyediting, typesetting, pagination and proofreading process which may lead to differences between this version and the Version of Record. Please cite this article as doi: 10.1002/fld.4813

1 Introduction

Interfacial flows are significant for numerous engineering applications and nature fields [1-3]. Smoothed particle hydrodynamics (SPH) is generally considered as an ideal solution for this problem [4]. The main reason is that there is no explicit interface tracking technology for the moving interfaces, and SPH has a great ability to large deformation interfacial problems. However, a conventional SPH formulation is difficult to maintain a stable interface, especially for problems with large density ratios (e.g., water-air flow with a typical density ratio of around 800 [5]). Since the pressure gradient for particles nearby the interface can introduce error due to the density discontinuous over the interface. Thus, SPH models for interfacial flows have been conducted by many researchers [6-10].

In 2003, some numerical algorithms were introduced by Colagrossi and Landini to stabilize interfacial flow simulations [5], including density renormalization, XSPH correction, large surface tension within the low-density phase and large artificial viscosity term. However, they did not consider surface tension . In 2006, an improved SPH discrete mode was represented by Hu and Adams based on particle number density [11]. However, no free surface problems were simulated in their work [11, 12]. Grenier et al. proposed another multi-phase SPH model for simulation of free surface problems [13]. In their work, the density was calculated from a standard SPH summation using a Shepard kernel, and the time-stepping algorithm was a fourth-order Runge–Kutta. Then, many multi-phase models were presented, including a simple model proposed by Monaghan and Rafiee [14], the one proposed by Chen et al. [15], a new two-phase incompressible-compressible proposed by Lind et al. [16]. However, they also did not consider either surface. In this paper, an integrated SPH formulation for simulating interface flows is proposed, which considers interfacial flow physical significance (e.g., various viscosity and surface tension). The model includes an improved continuity and acceleration equation discrete schemes, continuity continuum surface tension model and generalized multi-phase boundary condition. The artificial viscosity or δ-SPH item is not considered in this SPH model. In order to maintain numerical stability, interface particle shifting algorithms (Interface-PSA) is used here. Moreover, various numerical testes are simulated, including hydrostatic problems, droplet problems, Rayleigh-Taylor instability, dam breaking and bubble problems.

At first, the SPH discrete equation is rewrote based on particle number density and the Eckart's

Lagrangian equation [18] introduced by Springel and Hernquist[19], Monaghan [14]. The mass of particles is regarded as to be constant in this model and various fluid is supposed to be weakly compressible. Then a discrete formulation for the equation of continuity can be obtained by calculating the time derivative of the volume of particles. Subsequently, the acceleration equation can be derived by the Eckart's continuum Lagrangian equation and the discrete formulation for the equation of continuity. As only the summation of velocity and position information of nearby particles are used, it is totally suitable for interfacial flow problems.

For some typical interfacial problems, the surface tension is greatly important and should be not neglected. In the context of the SPH method, the continuum surface force (CSF) model in terms of macroscopic description firstly introduced by Brackbill et al. [20] was used widely [9, 17, 21-25]. In this method, a color function was applied to determine interfaces, and the gradient of color could be used to calculate the normal direction and curvature at the interface. Most current methods assumed that surface tension distributed uniformly, which results in numerical problems [26](e.g., air-water interface flow the surface force on the airside can introduce an acceleration about 1000 times higher than that on the waterside, the step-size for time integration is strongly limited). In 2010, a CSF formulation was used to correspond to the fact that the surface force may not be distributed uniformly on each side of the interface in realistic configurations by Adami et al. [26]. In our work, based on the assumption of the continuity of acceleration over the interface, an acceleration continuity CSF model is obtained, which has been tested accurately.

In the present formulation, an interface particle shifting algorithm (Interface-PSA) is paid to enhance the accuracy of the scheme, initially proposed by Xu et al. [27] to avoid anisotropic particle spacing. The algorithm involves slightly shifting the particles across streamlines thereby avoiding the extreme stretching and bunching of particles. This algorithm was improved by Lind et al. [28] using Fick diffusion and extended to free-surface flows. Since PSA can lead to better accuracy and stable for single-phase flows, it has been widely used [29-31]. As for interfacial flows, there are some recent works about PSA for multi-phase flows [9, 16, 28, 32]. One of the approaches is that the original PSA is directly used [to9, 16]. However, original PSA will cause interface unsmoothed according our simulations in Section 3. Another approaches are that PSA is used only for one of various flows [32]. Obviously, this approach can't fully exploit the advantages of PSA to each phase. Thus, we present an interface particle shifting algorithm, which is highly adapted to

interfacial flows. For various flow problems, wall boundary may be influenced by various fluid. Here, the improved density re-initialization introduced by Chen et al. [15] is used to make sure pressure equilibrium near the boundary. Meanwhile, free-slip or no-slip wall boundary conditions can be applied in our work.

The outline of the paper is as follows: governing equation is introduced firstly; then the interfacial SPH model and the discretization methods are presented in Section 3. Next, numerical results are presented in Section 4 to validate the model and show the accuracy and robustness of the proposed method by solving different benchmark problems. Finally, conclusions are drawn.

2 Governing Equation

In general isothermal conditions, the fluid behavior can be described by the Navier-Stokes equations in the Lagrangian framework

$$\frac{d\rho}{dt} = -\rho\nabla\cdot\boldsymbol{u}, \tag{1}$$

$$\frac{d\boldsymbol{u}}{dt} = -\frac{1}{\rho}\nabla p + \frac{\boldsymbol{F}_v}{\rho} + \frac{\boldsymbol{F}_s}{\rho} + \boldsymbol{g}, \tag{2}$$

where ρ, $\boldsymbol{u}$ and p are the density, velocity, and pressure of each particle, respectively. While $\boldsymbol{F}_v$, $\boldsymbol{F}_s$, $\boldsymbol{g}$ denote the viscous, the surface tension and the gravity forces.

In Lagrangian formalism, the location of a particle $\boldsymbol{X}$ at time t is obtained through

$$\frac{d\boldsymbol{X}}{dt} = \boldsymbol{u}. \tag{3}$$

For incompressible flow, the viscous force can be written as

$$\boldsymbol{F}_v = \nu\nabla^2\boldsymbol{u}, \tag{4}$$

where $\nu = \mu/\rho$ is the kinematic viscosity (μ denotes dynamics viscosity). In this work, the continued surface force (CSF) model of Brackbill et al. [20] is adopted, and the surface force can be expressed as a volumetric force

$$\boldsymbol{F}_s = -\beta\kappa\boldsymbol{n}\delta_\Sigma, \tag{5}$$

where β, κ and $\boldsymbol{n}$ are the surface tension coefficient, the interface curvature, and the interface unit normal vector. The surface-delta function δ_Σ is used to smooth the pressure-jump condition normal to an interface.

One common strategy in the SPH method is to assume the incompressible flow to be weakly compressible. Therefore, an equation of state is used to relate the pressure to density. This treatment avoids the tedious process of solving the pressure Poisson equation. Here, the isothermal equation

of state used in our work is expressed as

$$p = \frac{c_0^2 \rho_0}{\gamma}\left[\left(\frac{\rho}{\rho_0}\right)^{\gamma} - 1\right] + p_b, \tag{6}$$

where γ is different for various fluids (7 for heavier fluid and 1.4 for lighter fluid), the reference numerical sound speed c_0, the reference density ρ_0 and the background pressure p_b [5]. The numerical speed of sound is chosen following an analysis presented by Morris et al. [33] to approximate a constant-density fluid accurately, which leads to a very small time step. In our work, the numerical sound speed is determined by

$$c_0^2 \geq \max\left\{\frac{U_{max}^2}{0.01}, \ \frac{gH}{0.01}, \ \frac{\beta}{0.01\rho_0 H}\right\}, \tag{7}$$

where U_{max} and H are the maximum velocity and the undisturbed fluid depth. The above formulation aims to ensure that the variation of fluid density is less than 1% [34].

The pressure of particles may be less than zero in special circumstances, which is impractical. This leads to unphysical cavitations. Therefore, the background pressure p_b is used to prevent the occurrence of negative pressures, which should be restricted to the minimum value for stable simulation. In particular, the background pressures are different for various interfacial flows system [22, 35, 36].

Summarizing, the governing equations used in this work are

$$\begin{cases} \dfrac{d\rho}{dt} = -\rho\nabla\cdot\boldsymbol{u}, \\ \dfrac{d\boldsymbol{u}}{dt} = -\dfrac{1}{\rho}\nabla p + \dfrac{\boldsymbol{F}_v}{\rho} + \dfrac{\boldsymbol{F}_s}{\rho} + \boldsymbol{g}, \\ p = \dfrac{c_0^2\rho_0}{\gamma}\left[\left(\dfrac{\rho}{\rho_0}\right)^{\gamma} - 1\right] + p_b; \quad \dfrac{d\boldsymbol{X}}{dt} = \boldsymbol{u}. \end{cases} \tag{8}$$

3 Interfacial SPH Model

3.1 The continuity equation

A classical SPH density field approximated at the interface between two immiscible fluids can be written as

$$\rho_i = \sum_j \rho_j V_j W_{ij}. \tag{9}$$

It is obvious that the expression will lead to errors and unsteadiness at the interface due to the discontinuous density. To overcome this problem, the particle number density $n_i = \sum_j W_{ij}$ is

introduced here. The particle number density was firstly proposed for two-dimensional incompressible non-viscous flow analysis using the moving particle semi-implicit (MPS) method [37]. It is found that n_i has a larger value in a dense particle region than in a dilute particle region. In 2006, Hu and Adams [11] proposed a density field approximated using the particle number density

$$\rho_i = \rho_i \sum_j V_j W_{ij}. \tag{10}$$

The difference between Eq. (9) and Eq. (10) is that in Eq. (10) neighboring particles contribute to the particle density only by affecting the specific position and volume of particle i. In other words, Eq. (10) allows for density discontinuities when there are large particle density differences between nearby particles. A smoothing function is introduced firstly

$$\mathbb{W}_{\mathrm{i}}(\boldsymbol{r}) = \frac{W_{ij}}{\sum_k W_{ik}}, \tag{11}$$

where $\boldsymbol{r}$ is the position of a particle, k is the number of all neighbor particles (including different phase particles). Then the volume of a particle through the integral over the entire domain can be obtained

$$V_i = \int \frac{W_{ij}}{\sum_k W_{ik}} dr = \frac{\Gamma_i}{\sum_k W_{ik}} = \frac{1}{N_i} \quad \left(\Gamma_i = \int W_{ij} dr\right). \tag{12}$$

In SPH, particles tend to follow accurately the fluid flow trajectories, leading to the presence of anisotropic particle structures. Actually, $\Gamma_i = \int W_{ij} dr \neq 1$(especially, near the boundary domain in multi-phase flow and disorder particle domain). Thus, we can reconsider the formulation as

$$V_i = \int \mathbb{W}_i(\boldsymbol{r})\, d\boldsymbol{r} = \frac{\Gamma_i}{N_i}. \tag{13}$$

It is found that the Shepard correction is used here, which can increase the order of convergence of the interpolation [1, 11, 13, 38-40]. At the same time, the formulation recovers an accurate volume at the regions close to boundary due to the absence of points on the other side of this boundary.

As a Lagrangian particle method, SPH conserves mass exactly. And in our work, the interfacial flows are considered to be weakly-compressible. This means that the volume of a particle is non-constant. Then using the accuracy volume of a particle in Eq. (13), the time derivative of particle volume is obtained as

$$\frac{d}{dt}\frac{1}{V_i} = \sum_j \frac{1}{\Gamma_i}\frac{dW_{ij}}{dt} + \frac{N_i}{\Gamma_i^2}\frac{d\Gamma_i}{dt}. \tag{14}$$

Even though Γ_i is not always equal to 1, the change of Γ_i in each small time step can be almost zero. the second term on the right-hand side of Eq. (14) is disregarded. Consequently, we can have

$$\frac{d}{dt}\frac{1}{V_i} = \sum_j \frac{1}{\Gamma_i}(\boldsymbol{u}_i - \boldsymbol{u}_j)\cdot\nabla W_{ij}. \tag{15}$$

Considering a direct relationship between the particle mass m_i, density and elementary volume V_i that is assumed (i.e. $\rho_i = m_i/V_i$), a discrete formulation of the continuity equation is obtained as

$$\frac{d}{dt}\rho_i = \mathrm{m}_i \sum_j \frac{1}{\Gamma_i}(\boldsymbol{u}_i - \boldsymbol{u}_j)\cdot\nabla W_{ij}. \tag{16}$$

It is found that the velocity and position information of nearby particles is uniquely considered here. That means that this discrete formulation is suitable for interfacial problems with big density ratios. At the same time, Shepard correction is used here to improve accuracy. The summation for calculating the term Γ_i is extended to all particles belonging to different phase flows. It is different from the summation introduced by Grenier et al. [13], which considers the summation in different phases.

3.2 The acceleration equation

In principle, it is possible to construct Lagrangian treatments of hydrodynamics that behave better in their conservation properties [19]. Following Monaghan et al.' work, the Lagrangian-based SPH acceleration equation can be derived by Eckart's continuum Lagrangian equation [41]. It is assumed that the pressure in each phase flow can be found from an internal energy ε that may have a different functional form for each fluid. The effects of surface tension, viscous force, and boundary force are neglect here. Besides that, the entropy for each particle is set to be constant the entire time. The Lagrangian for compressible, non-dissipative flow is

$$L = \int \rho\left(\frac{1}{2}\boldsymbol{u}\cdot\boldsymbol{u} - \varepsilon(\rho, s)\right)d\boldsymbol{r}. \tag{17}$$

Hence, the SPH Lagrangian equation for a particle i is obtained

$$\mathrm{L} = \sum_j m_j\left(\frac{1}{2}\mathbf{u}_j^2 - \varepsilon_j(\rho_j)\right). \tag{18}$$

Following Monaghan' work [14], the acceleration equation for particle i can results from theLagrangian equation

$$\frac{d}{dt}\left(\frac{\partial L}{\partial \mathbf{u}_i}\right) = \frac{\delta L}{\delta \boldsymbol{r_i}}, \tag{19}$$

where δ denotes a Lagrangian change. It is found that

$$\frac{\delta L}{\delta \boldsymbol{r_i}} = -\sum_j m_j \left(\frac{d\varepsilon(\rho_j)}{d\rho_j}\right)\frac{\delta \rho_j}{\delta \boldsymbol{r}_i}. \tag{20}$$

According to the first law of thermodynamics

$$\frac{d\varepsilon_j(\rho_j)}{d\rho_j} = \frac{P_j}{\rho_j^2}. \tag{21}$$

The relation between Lagrangian equation changes in density and coordinates follows from the continuity Eq. (16). Thus, we can deduce that

$$\frac{\delta \rho_j}{\delta \boldsymbol{r}_i} = m_j \sum_k \left(\frac{\delta_{ji}}{\Gamma_j} - \frac{\delta_{ki}}{\Gamma_i}\right)\nabla_j W_{jk}, \tag{22}$$

where δ_{ji} is a Kronecker delta, which is 0 if $i = j$ and 1 otherwise. Substitution of Eq. (22) into Eq. (20) gives

$$\frac{\delta L}{\delta \boldsymbol{r}_i} = -V_i^2 P_i \sum_k \frac{1}{\Gamma_i}\nabla_i W_{ik} + \sum_j \frac{1}{\Gamma_j} V_j^2 P_j \nabla_j W_{ji}. \tag{23}$$

Finally, the acceleration equation can be obtained

$$\frac{d\mathbf{u}_i}{dt} = -\frac{1}{m_i}\sum_j \left(\frac{V_i^2 P_i}{\Gamma_i} + \frac{V_j^2 P_j}{\Gamma_j}\right)\nabla_i W_{\mathrm{ij}}. \tag{24}$$

It can be found that the summation for particle i just considers the volume, position, and pressure of these particles in its support domain, even for different phase particles. According to Chen's work [15], pressure can be seen as continuity over the interface. Thus, we can define that Eq. (24) is applicable for interfacial flows with big density ratios. More validation cases are simulated in Section 4.

Regarding the viscous force, the formulation proposed by Monaghan and Gingold [42] can be adopted in the present model. While the dynamic viscous coefficient needs an adjustment on the multiphase interface for multiphase flows. Here, $\mu_{ij} = 2\,\mu_i\mu_j/(\mu_i + \mu_j)$ proposed by Hu and Adams [11] is used, where i and j denote the particles of different phases, and then the viscosity forces can be expressed as

$$\boldsymbol{F}_v = \sum_j \xi \frac{2\mu_i\mu_j}{\mu_i + \mu_j}\frac{(\boldsymbol{u}_i - \boldsymbol{u}_j)\cdot(\boldsymbol{r}_i - \boldsymbol{r}_j)}{|\boldsymbol{r}_i - \boldsymbol{r}_j|^2 + (\epsilon h)^2} V_j \nabla_i W_{ij}, \tag{25}$$

where $\xi = 2(n+2)$, which depends on the spatial dimension n [22].

3.3 Continuum Surface Force Model (CSF)

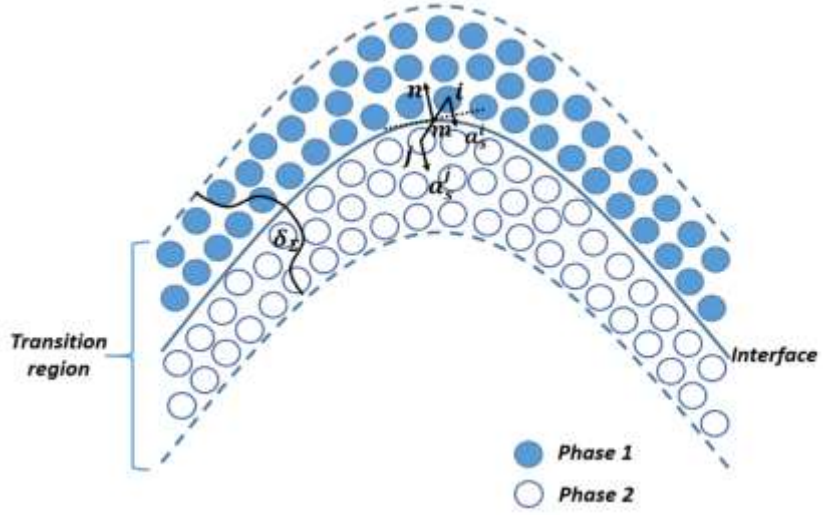

Fig.1. Sketch of the transitional domain near the multiphase interface.

The surface tension is important and should be not neglected as some typical interfacial flow problems. In order to calculate surface-tension forces between particles of different phases, a color function is firstly introduced here

$$c_i = \begin{cases} 1 & if\ particle\ i\ \ belongs\ to\ \ phase\ 1 \\ 0 & if\ particle\ i\ \ belongs\ to\ \ phase\ 2 \end{cases}. \tag{26}$$

Note that, this color function has a unit-jump at a phase interface, which fits multi-phase problems well. Generally, $|\nabla c_i|$ is regarded as a surface-delta function δ_Σ, as the gradient of the color function has a delta-function-like distribution. Thus, we can obtain the surface tension of particle i over the interface as

$$\boldsymbol{F_s^i} = -\beta\kappa\boldsymbol{n}\delta_\Sigma = \beta(\nabla\cdot\boldsymbol{n})\nabla c_i. \tag{27}$$

For most existing CSF model, the surface tension force distributes uniformly on each side of the interface. It's not a realistic configuration. For example, at an air-water interface, the surface force is dominantly acting on the waterside. Besides that, an air-water interface flow the surface force on the airside can introduce an acceleration about 1000 times higher than that on the waterside, the step-size for time integration is strongly limited [26]. Thus, we assume the continuity of acceleration of surface tension across the interface. If that, the surface tension will distribute uniformly for interfacial flows with big density ratios. Considering particle i and particle j nearby the interface belongs to different phases, one can assume that the phase interface is located at the center m between particle i and j, as shown in Fig.1. In his way, we can have the continuity of acceleration

$$\boldsymbol{a}_s^i = \frac{\beta(\nabla\cdot(\nabla c_{im}/|\nabla c_{im}|))\nabla c_{im}}{\rho_i} = \frac{\beta(\nabla\cdot(\nabla c_{mj}/|\nabla c_{mj}|))\nabla c_{mj}}{\rho_j} = \boldsymbol{a}_s^j. \tag{28}$$

Then, we can have

$$\frac{\nabla c_{\mathrm{im}}}{\rho_i} = \frac{\nabla c_{mj}}{\rho_j}, \tag{29}$$

where $\nabla c_{im} = c_i - c_m, \nabla c_{mj} = c_m - c_j$. Then, we can get the continuity color coefficient

$$c_m^{ij} = \frac{c_j\rho_i + c_i\rho_j}{\rho_i + \rho_j}. \tag{30}$$

Noted that, if particle i and particle j belong to phase 1, $c_m^{ij} = 1$; if particle i and particle j belong to phase 2, $c_m^{ij} = 0$, if particle i and particle j belong to different phases, $c_{ij}^m \in [0,1]$. Thus, Eq. (30) can also be expressed as

$$c_m^{ij} = \begin{cases} 1 & i\ and\ particle\ j\ belong\ to\ phase\ 1 \\ \dfrac{c_j\rho_i + c_i\rho_j}{\rho_i + \rho_j} & i\ and\ particle\ j\ belong\ to\ different\ phases. \\ 0 & i\ and\ particle\ j\ belong\ to\ phase\ 2 \end{cases} \tag{31}$$

Above density-weighted color coefficient c_m^{ij} is totally appropriate for the whole interfacial flow system. Usually, the gradient of color ∇c_i is calculated as

$$\nabla c_i = \sum_j (c_j - c_i)\nabla W_{ij}V_j. \tag{32}$$

It is a common formulation based standard SPH interpolation. Specially, c_j is replaced with c_m^{ij} to ensure the continuity of acceleration here. As shown in Eq. (32), when considering different fluids, density-weighted color coefficient c_m^{ij} is totally appropriate for the various flows system. Moreover, the kernel gradient correction is applied to improve accuracy. Then we have

$$\nabla c_i = \sum_j 2\left(c_m^{ij} - c_i\right)\boldsymbol{M}\nabla W_{ij}V_j = \sum_j 2\frac{(c_j - c_i)\rho_i}{\rho_i + \rho_j}\boldsymbol{M}\nabla W_{ij}V_j, \tag{33}$$

where $\boldsymbol{M} = \left[\sum_j (\boldsymbol{r}_j - \boldsymbol{r}_i) \otimes \nabla W_{ij}V_j\right]^{-1}$. In order to compare with Adami et al. 's work [26], we list the gradient of their color function as following

$$\begin{cases} \nabla c_i = \dfrac{1}{V_i}\displaystyle\sum_j (V_i + V_j)\left(\frac{\rho_j}{\rho_i + \rho_j} C_i^i + \frac{\rho_i}{\rho_i + \rho_j} C_j^i\right)\nabla W_{ij} \\ C_j^i = 1 \quad if\ i\ \ and\ j\ belong\ to\ the\ different\ phases \\ C_j^i = 0 \quad if\ i\ and\ j\ belong\ to\ the\ same\ phase \end{cases}, \tag{34}$$

It can be found that Eq. (33) and Eq. (34) have a similar formulation. Hence, the above derivation process suggests that the formulation proposed by Adami et al. [26] meets the assumption of acceleration continuity in part. Then, the normal unit vectors $\boldsymbol{n}$ can be calculated using the formulation

$$\boldsymbol{n}_i = \frac{\nabla c_i}{|\nabla c_i|}. \tag{35}$$

Then curvature κ_i is calculated as follows:

$$\kappa_i = -\nabla \cdot \boldsymbol{n_i} = -\sum_j (\boldsymbol{n}_j - \boldsymbol{n}_i)\boldsymbol{M}\nabla W_{ij}\Delta V_j. \tag{36}$$

In the CSF model, the interface is the region where the color coefficient changes significantly. Usually, large errors will occur at the fringes of the transition zone [21]. The main reason is that ∇c is quite small and will lead an erroneous normal unit vectors $\boldsymbol{n}$ under some circumstances. As a result, any estimate of curvature that uses these normal direction will be inaccurate. The efficient solution is filtering as suggested in, i.e.

$$\kappa_i = \begin{cases} -\nabla \cdot \boldsymbol{n}_i & |\boldsymbol{n}_i| > 0.01 \\ 0 & |\boldsymbol{n}_i| \le 0.01 \end{cases}. \tag{37}$$

3.4 Boundary condition

In this work, we improve the wall boundary condition method proposed by Chen et al. [15] to deal with two-phase fluid flows. In this method, three layers of dummy particles must be added in the normal direction to the wall interface, and the reference density of dummy particles can be set to the same value with the one of heavier fluid. The dummy particles are placed to represent the wall in such a way that it is ensured the completeness of the support of kernel function, in order to obtain an accurate integration of the field variables near the wall interface.

Free-slip or no-slip wall boundary conditions can be applied using this method. For free-slip and no-slip conditions, the normal component of the fluid velocity is reversed to guarantee the boundary condition

$$\boldsymbol{u_d} \cdot \boldsymbol{n_w} = -\boldsymbol{u_d} \cdot \boldsymbol{n_w}, \tag{38}$$

where $\boldsymbol{u_d}$ is the velocity of dummy particles and $\boldsymbol{n_w}$ is the normal direction of the wall, respectively. If wall velocity is an explicit value, the free-slip boundary condition is applied by maintaining prescribed wall velocity

$$\boldsymbol{u_d} \cdot \boldsymbol{\tau_w} = \boldsymbol{u_w} \cdot \boldsymbol{\tau_w}\,, \tag{39}$$

where $\boldsymbol{u_w}$ denotes the prescribed wall velocity and $\boldsymbol{\tau_w}$ denotes the tangent direction of the wall, respectively. Otherwise, the dummy particle velocity can be determined by

$$\boldsymbol{u_d} = \frac{\sum_q \boldsymbol{u}_q W_{dq} + \sum_l \boldsymbol{u}_l W_{dl}}{\sum_b W_{db}}\,, \tag{40}$$

where $\boldsymbol{u}_q$ and $\boldsymbol{u}_l$ denote the velocity of fluid particles belonging to phase q and l.In the case of no-slip wall boundary condition, a virtual velocity is imposed on the wall-dummy particle. This velocity is defined as

$$\boldsymbol{u}_d \cdot \boldsymbol{\tau_w} = 2 * \boldsymbol{u_w} \cdot \boldsymbol{\tau_w} - \boldsymbol{u_d} \cdot \boldsymbol{\tau_w}\,. \tag{41}$$

A generalized and simple method which is used to determine normal directions of the wall is used here

$$\boldsymbol{n_w} = \frac{\sum_{j\in f} \nabla W_{jf} V_j}{\left|\sum_{j\in f} \nabla W_{jf} V_j\right|}\,, \tag{42}$$

where $j \in f$ denotes all neighbor fluid particles in the support domain.

For interfacial flow problems, the dummy particles may interact with various fluid particles in its support domain, as shown in Fig.2. All these particles are required to be paid the same attention. When calculating the density of dummy particles, density oscillation and errors will be lead due to the density-discontinuity. It is important to include the acceleration of the wall when computing the boundary pressure [43]. Therefore, an improved density re-initialization by Chen et al. [15] is introduced to calculate the pressure of dummy particles nearby the interface here

$$p_d = \frac{\sum_q p_q W_{dq} V_q + \sum_l p_l W_{dl} V_l + (\boldsymbol{g} - \boldsymbol{a_w}) \sum_q \rho_q \boldsymbol{r}_{dq} W_{dq} V_q + (\boldsymbol{g} - \boldsymbol{a_w}) \sum_l \rho_l^* \boldsymbol{r}_{dl} W_{dl} V_l}{\sum_b W_{db} V_b}, \tag{43}$$

$$\rho_l^* = \frac{(p_l - p_0)}{c_{l0}^2} + \rho_{l0}, \tag{44}$$

where ρ_d, ρ_{l0}, $\boldsymbol{a_w}$ and c_{l0} are the density of dummy particles, reference higher density of particle l, acceleration of the wall and the reference numerical speed for phase l, respectively. Then, the density of the dummy particle can be obtained as

$$\rho_d = \frac{(p_d - p_0)}{c_{d0}^2} + \rho_{d0}, \tag{45}$$

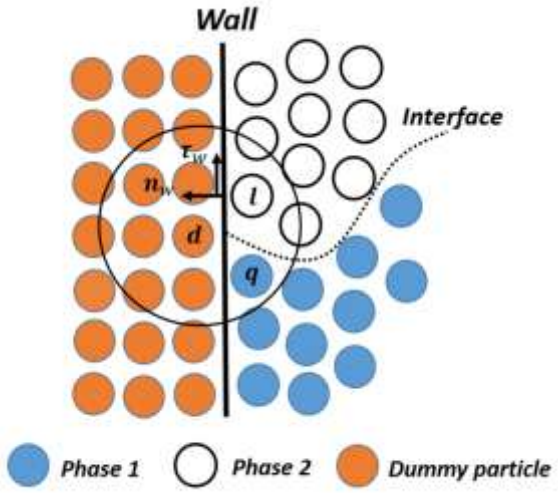

Fig.2. Illustration of wall boundary treatment.

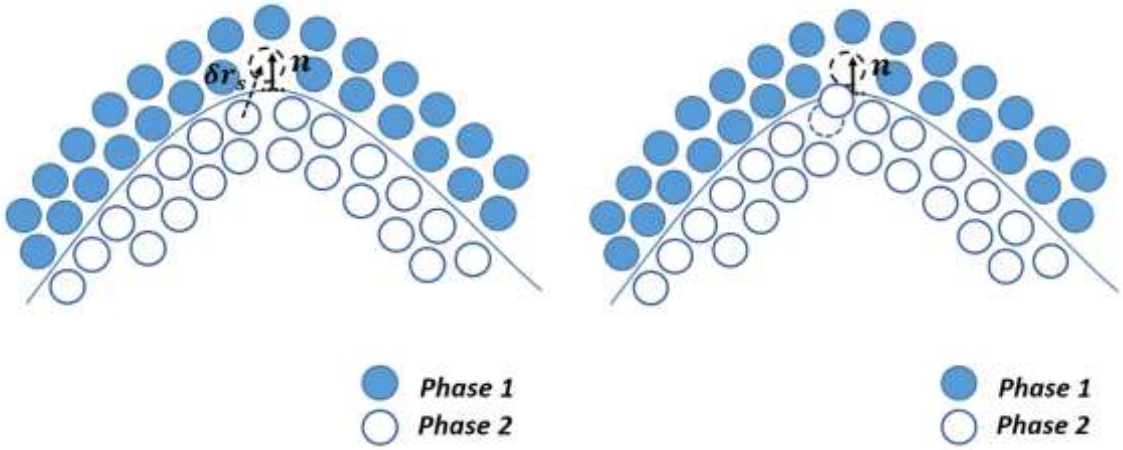

Fig.3. Illustration of particle shifting with original PSA

3.5 Interface particle shifting algorithm (Interface-PSA)

The particle shifting scheme is founded on Fick's diffusion law and relies on a Taylor expansion for evaluation of particle quantities in the new position [27, 28]. Since PSA has been widely used for the advantage of better accuracy and stable for single-phase flows. The effectiveness of this scheme has been shown in a number of papers [29, 31, 44]. However, when modelling two-phase flows by the original PSA, some problems may happen, as shown in Fig. 19. Thus, we improve PSA for two-phase flows in this section.

We firstly introduce the original PSA. In PSA, the Fick's law is expressed as:

$$\boldsymbol{J} = -\mathcal{D}\nabla\mathbb{C}\,, \tag{46}$$

where $\boldsymbol{J}$ is the diffusion flux, $\mathcal{D}$ is a diffusion coefficient and $\mathbb{C}$ is the concentration. $\boldsymbol{J}$ corresponds to

the number of particles passing through a unit surface in unit time, which is proportional to the particle shifting velocity $\boldsymbol{u}_s$. Thus, the particle displacement vector is written as:

$$\delta \boldsymbol{r}_s = -D' \nabla \mathbb{C}', \tag{47}$$

where D' is a new diffusion coefficient, $\mathbb{C}'$ is the particle concentration. The particle concentration and its gradient can be calculated as follow:

$$\mathbb{C}_i = \sum_j V_j W_{ij} \ , \tag{48}$$

$$\nabla \mathbb{C}_i = \sum_j V_j \nabla W_{ij} \ . \tag{49}$$

Considering the CFL condition for a specific velocity and particle spacing, the particle shifting displacement vector $\delta \boldsymbol{r}_i$ for particle, i is obtained as

$$\delta \boldsymbol{r}_s = -Ah \|\boldsymbol{u}_i\| \nabla \mathbb{C} \Delta t \, , \tag{50}$$

where A is a problem-independent dimensionless constant (Here, $A = 2$). Finally, the hydrodynamic variable (density, pressure, and velocity) should be corrected by Taylor series approximation

$$\phi_{i\prime} = \phi_i + (\nabla \phi)_i \cdot \delta \boldsymbol{r}_{ii'} + o(\delta \boldsymbol{r}_{ii'}{}^2) \, . \tag{51}$$

Although PSA shows the excellent performance in single-phase simulation, there exist some problems when used in multi-phase problems. In 2016 and 2017, PSA has been applied to multi-phase flows by Lind et al. [16] and Mokos et al. [32]. However, PSA is used in one phase of various phases. In this section, PSA is improved for the whole two-phase system. According to our research, PSA in interfacial flows should pay attention to some following details:

(a) The particle concentration is also suitable for interfacial flows. According to the particle number density, the volume and position of particles for the different phases are continuous. Therefore, the measure of particle concentration and its gradient fit multi-phase flow with a big density radio. For interfacial SPH, there is no large concentration gradient at the free surface thanks to the different phase particle filling the entire computational domains. Thus, PSA should be suitable for the interfacial SPH model.

(b) The particle shifting displacement should be restricted at the interface. Due to the same measure of concentration for different phase particles, a particle shifting near the interface will be corrected willfully. Consequently, the particle shifting for the particles at

the interface will lead to some errors and oscillation for the interface, as shown in Fig.3. Seriously, unphysical particle penetration will happen. In order to solve this problem, the interface normal shifting displacement should be forbidden. It means that particles will slightly shift along the tangential direction of the interface, as shown in Fig.5. Then, the particle shifting displacement can be finally written as

$$\delta \boldsymbol{r}_s' = \delta \boldsymbol{r}_s - \delta \boldsymbol{r}_s^n = \delta \boldsymbol{r}_s - \frac{\nabla c}{|\nabla c|} \cdot \delta \boldsymbol{r_s} = \delta \boldsymbol{r}_s^\tau . \tag{52}$$

Here, the interface normal direction can be determined by the gradient of the color coefficient. Far from the interface, $\boldsymbol{n} = 0$. Actually, forbidding the interface normal shifting displacement means that the gradient of particle concentration in the normal direction is ignored. Even for the same formulation with previous work [29, 30], the Eq. (53) is essentially different from previous work. The correction normal direction in [29, 30] is as following

$$\begin{cases} n_i = \dfrac{\nabla \lambda_i}{|\nabla \lambda_i|} \quad \nabla \lambda_i = -\sum_j (\lambda_j - \lambda_i) M_i \nabla W_{ij} V_j \\ n_i = \dfrac{\nabla \mathcal{C}_i}{|\nabla \mathcal{C}_i|} \quad \nabla \mathcal{C}_i = -\sum_j M_i \nabla W_{ij} V_j \\ \lambda_i = the\ value\ of\ the\ minimum\ eigenvalue\ of\ \boldsymbol{M^{-1}} \end{cases} . \tag{53}$$

It's obtained that $\nabla \lambda_i$ or $\nabla \mathcal{C}_i$ is not strictly null inside fluid as the distribution of irregular particles. Thus, we can find the correction in their work is limited to these particles near the free surface. However, present formulation obtained by Eq. (35) has the following characters

$$\nabla c_i = \begin{cases} 0 & inside\ phase\ 1 \\ \sum_j 2 \dfrac{(c_j - c_i)\rho_i}{\rho_i + \rho_j} \boldsymbol{M} \nabla W_{ij} V_j & nearby\ the\ interface \\ 0 & inside\ phase\ 2 \end{cases} . \tag{54}$$

Thus, the modified shifting displacement $\delta \boldsymbol{r}_s'$ can be used to move particles in the whole interfacial flow calculation domain.

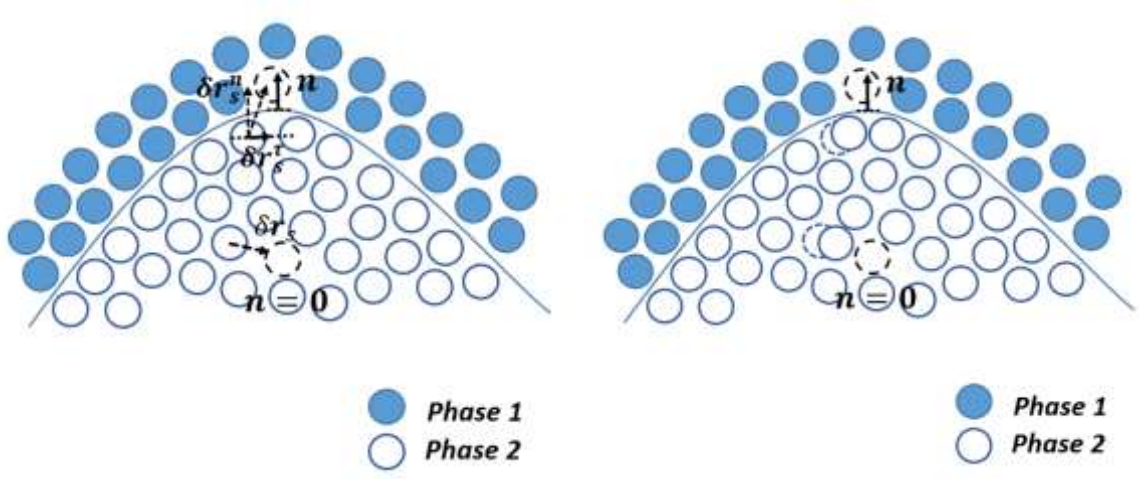

Fig.4. Illustration of particle shifting with interface-PSA.

(c) Because of the discontinuous physical qualities, correcting hydrodynamic variables (density, pressure, velocity and so on) should be modified. Considering density correct

$$\rho_{i\prime} = \rho_i + (\nabla\rho)_i \cdot \delta\boldsymbol{r}_{ii\prime}^{\tau} + o\left(\delta\boldsymbol{r}_{ii\prime}^{\tau\,2}\right). \tag{55}$$

$$(\nabla\rho)_i = \sum_j (\rho_j - \rho_i) V_j \nabla W_{ij}\ . \tag{56}$$

If particle i nearby the interface, the gradient of density is huge for multiphase flow with big density ratios. Consequently, though a light displacement $\delta\boldsymbol{r}_{ii'}$, the corrected density is totally different from previous density. Thus, a discontinuous SPH discretization scheme is introduced here for calculating the gradient of the discontinuous variable

$$(\nabla\rho)_i = \sum_{j\in S} (\rho_j - \rho_i) V_j \nabla W_{ij}\,. \tag{57}$$

where S denotes that particle j is the same phase with particle i.

In the present simulation, a prediction-correction time-stepping scheme is applied to ensure second-order accuracy. Moreover, in order to ensure numerical stability, the maximum time-step is chosen based on several criteria [45, 46]. Here, the time step must be constrained by the Courant-Friedrichs-Lewy (CFL) condition based on the artificial sound speed c_0:

$$\Delta t \le \frac{h}{c_0}, \tag{58}$$

the viscous diffusion condition:

$$\Delta t \le 0.125\frac{h^2}{\nu}, \tag{59}$$

and the body force condition:

$$\Delta t \leq 0.25\sqrt{\frac{h}{g}}, \tag{60}$$

and the surface tension condition

$$\Delta t \leq 0.25\sqrt{\frac{\rho h^3}{2\pi\beta}}, \tag{61}$$

For satisfying all conditions, the global time-step is taken as the minimum of Eq. (58-61).

4 Numerical Examples

4.1 Dam breaking

The dam breaking problem is a typical benchmark for testing free surface or multiphase flows as its violent impact and complex interface. Comprehensive analytical, numerical and experimental data are available for the validation of new numerical models [5, 16, 47, 48]. Here air-water two-phase flows with a water to air density ratio of around 800 are simulated. The initial width and height of the water column Ω_1 with the reference density of $1000\ \mathrm{kg/m^3}$ is L and H, as shown in Fig.5. While air phase Ω_2 with the reference density of $1.29\ \mathrm{kg/m^3}$ is at rest in the rectangular computational domain. The width and height of the computational domain are $5.366H$ and $3H$, respectively. The dynamics viscosity of water and air are $1.1\times10^{-3}\ \mathrm{kg/m\cdot s^{-1}}$ and $1.78\times10^{-5}\ \mathrm{kg/m\cdot s^{-1}}$, respectively. The pressure sensor locates on the right wall (0.06 m higher than the bottom of the container). And all walls meet no-slip boundary condition. A positive background pressure is taken as $p_b = 1200$ Pa.

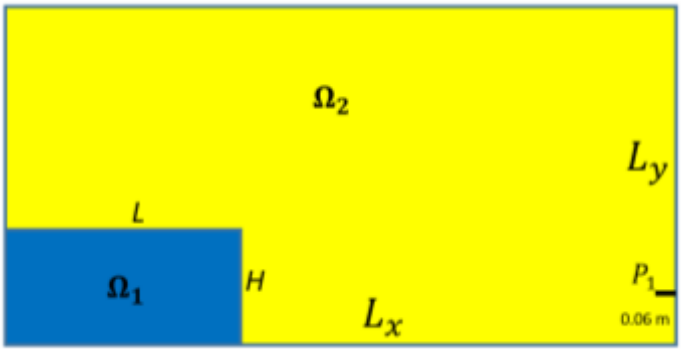

Fig.5. Illustration of the initial dam breaking model.

For a water column of dimension $H \times L = 0.3\ \mathrm{m} \times 0.3\ \mathrm{m}$, Fig.6 shows the evolution of the waterfront (the toe position) with time and comparisons with a single-phase boundary element method (BEM) [49] and Level set [5]. When the initial particle space is smaller than 0.02 m,

increasing the total number of particles does not significantly change the simulation results. This means that the obtained simulation results arrive at a convergent solution. Meanwhile, it can be found that Interface-PSA has no significant influence on the toe position. The main reason is that particle position correction near the interface is limited. Hence, Interface-PSA should be limited influence on interface position. In the following case, similar conclusion can be obtained.

For a slightly different water column geometry $H \times L = 0.3 \times 0.6$ m, Fig.7 compares the flow profiles of present SPH model with the single-phase boundary element method (BEM) [5] and two-phase level-set method [5] at $t\sqrt{g/H} = 5.95$ and $t\sqrt{g/H} = 6.75$. The air phase is not pictured for the purpose of clarity. The role of the air phase is still less important at this point in the flow, and the two-phase results for the water surface are in reasonable agreement with reference single-phase results.

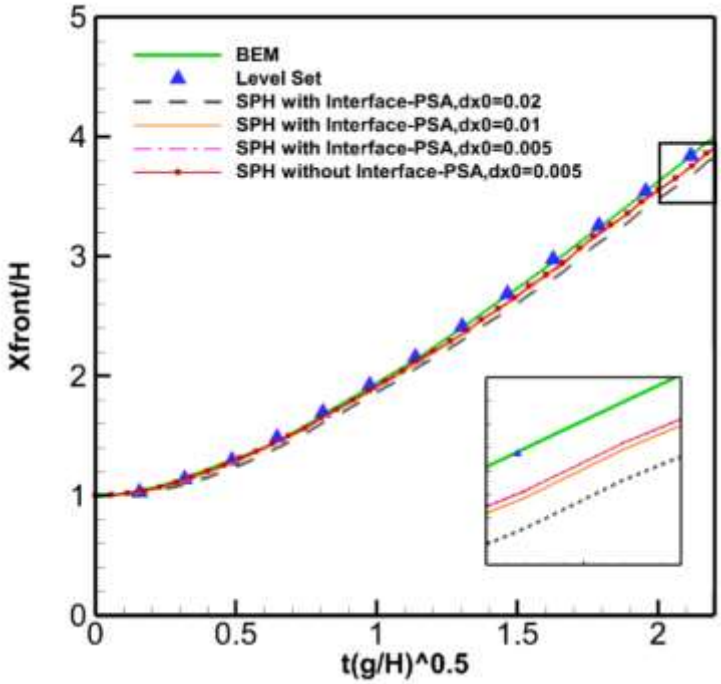

Fig. 6.The evolution of the waterfront (the toe position) for water column $H \times L = 0.3$ m $\times$ 0.3 m.

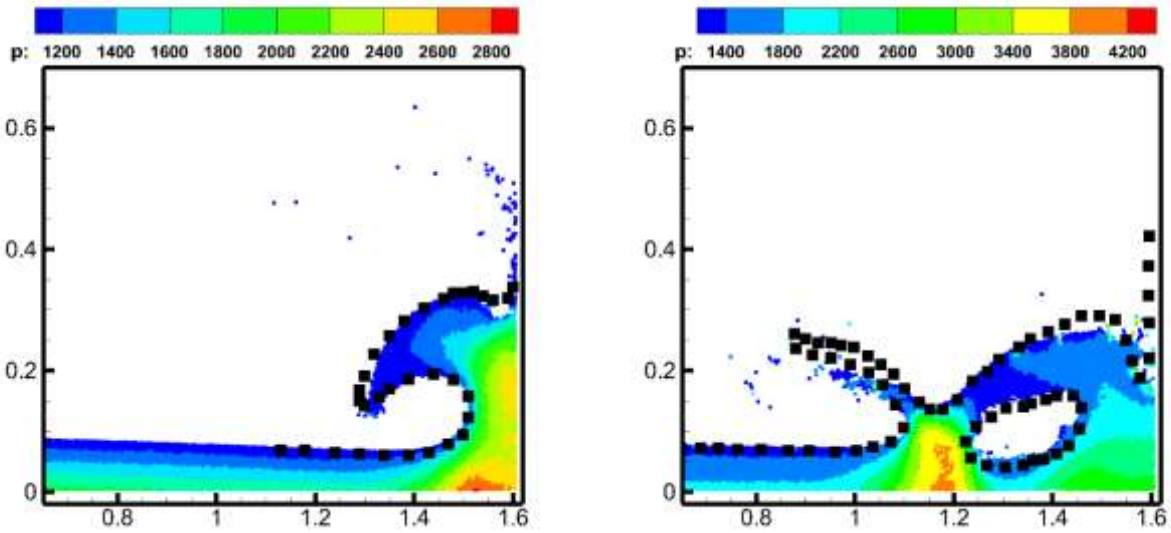

Fig.7.Comparisons of the fluid profile of the water phase with other numerical studies. (a) Comparison with a BEM study (black squares) at $t\sqrt{g/H} = 5.95$ [49]; (b) Comparison with a two-phase level-set study (black squares) at $t\sqrt{g/H} = 6.75$.

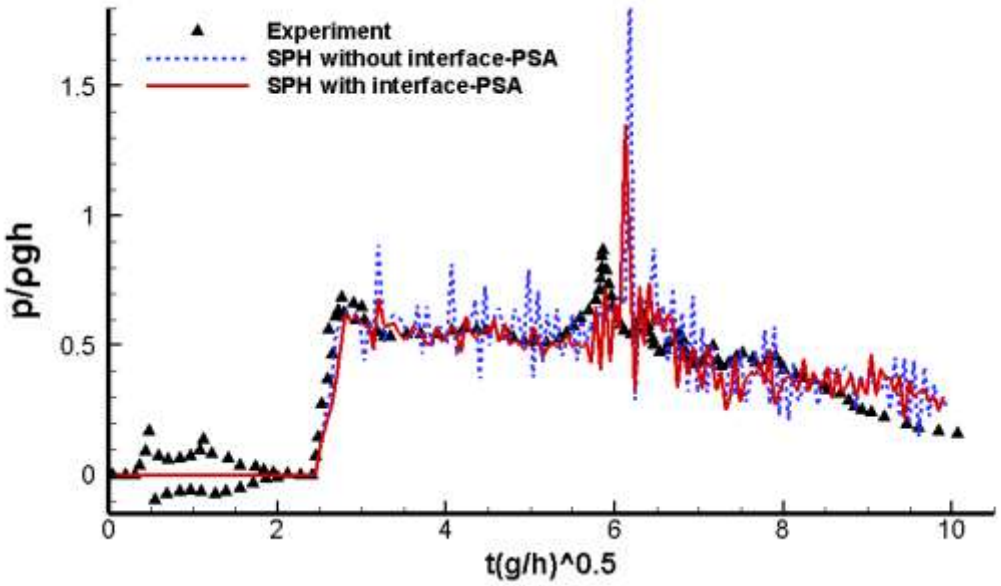

Fig.8.Time history of pressure on sensor compared with experimental data [50].

Fig.8 presents pressure measurements for the present SPH model with and without interface-PSA and experimental results from Zhou et al. [50]. The present interfacial SPH model compares well with experimental results. It can be seen two pressure peaks at approximate $t\sqrt{g/H} = 2.7$ and $t\sqrt{g/H} = 6.0$. At the same time, it also demonstrates present boundary conditions can calculate boundary pressure well. It is shown that pressure on the sensor with Interface-PSA has fewer oscillations before the second pressure peaks. There is less over-prediction of the secondary

pressure peaks. And after secondary pressure peaks, the pressure with Interface-PSA has also fewer oscillations compared with the results without Interface-PSA.

The main reason for oscillation after the second pressure is that some air particles are entrapped around the plunger tip when impinging on the underlying layer of water, which is called air cushion entrapment. In our model, the air phase is considered weakly-compressible fluids. In practical, the air entrapment in the plunging wave is compressible. Thus, the air phase will hold up great pressure resulting in slow decay, over-prediction of pressure and oscillations after the second pressure peak, as shown in Fig.9. Similar results can be found in previous work.

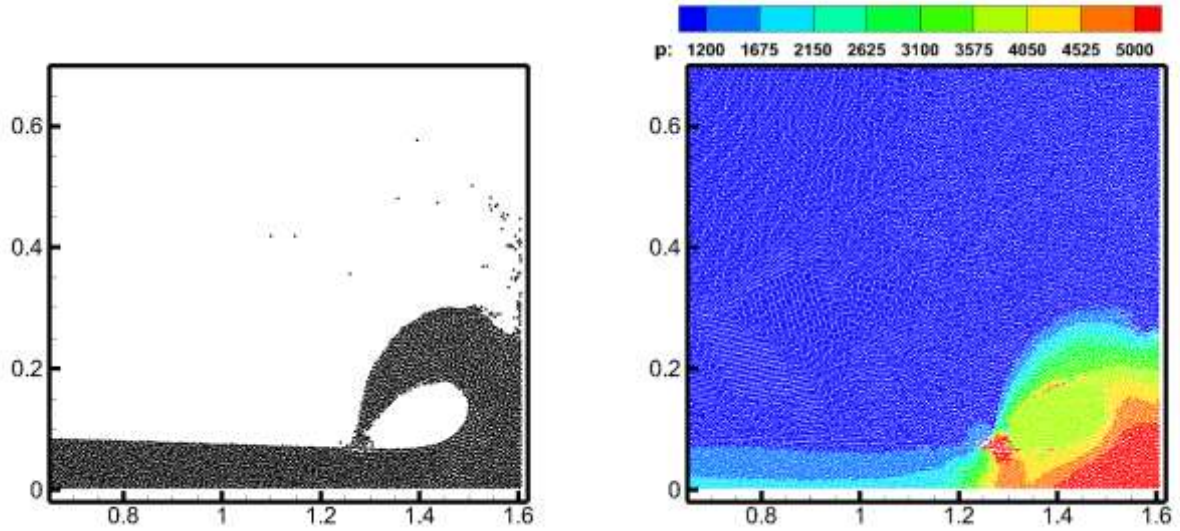

Fig.9.Water configuration and pressure field (both air and water phase) at $t\sqrt{g/H} = 6.1$.

4.2 Droplet deformation

In this case, the present interfacial SPH model is applied to the simulation of the deformation of a square droplet, which is devoted to the validation of the formulation for the surface tension mode and its ability to simulate multi-phase flow with big density ratios [21, 26, 51-53]. The square droplet with an initial edge length $L_a = 0.04$ m is placed on the center of a square box with side length $L_s = 0.2$ m. The fluid within the square droplet is referred to as phase 1, whereas the fluid outside the droplet is referred to as phase 2, as shown in Fig.10. The densities of each fluid phases are chosen as $\rho_1 = 1000\ \mathrm{kg/m^3}$ and $\rho_2 = 1\,\mathrm{kg/m^3}$, and the dynamic viscosity is taken as $\mu_1 = 0.2$ Pa. s and $\mu_1 = 0.02$ Pa. s. The surface tension coefficient is $\beta_1 = \beta_2 = 1\,\mathrm{N/m}$.

We investigate the evolution of square droplet using three different number of particles: $l_s/50$ $l_s/100$ and $l_s/200$. The reference speed of sound is set to $c_1 = 20$ and $c_2 = 10$ for all simulations. A positive background pressure is taken as $p_b = 90$ Pa.

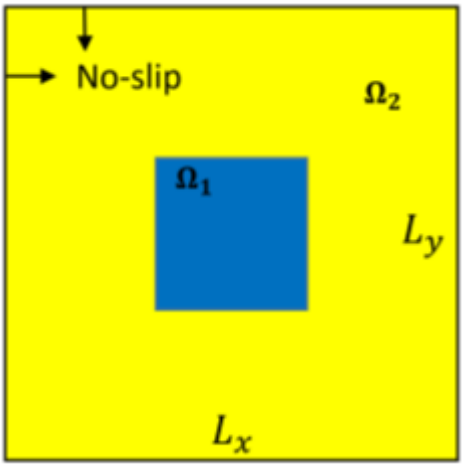

Fig.10. Illustration of the initial square-droplet model.

Fig. 11 shows the snapshots of shape evolution, the pressure field and velocity field of 2D initial square droplet for particle resolution $l_s/100$. Particles at the corner have pressure and velocities towards the center of the liquid square, firstly, as they have maximum curvature. Although the drop shape is similar at t=0.25 s and t=0.4 s, the particles have opposite speed, which indicates that drop is not at equilibrium. The 2D liquid drop evolves into in equilibrium at $t = 2.0$ s. At the moment, the pressure inside the droplet remains stable, and all fluid particles are almost motionless.

From Laplace's law, the pressure of the fluid particles inside the droplet (phase 1) is higher than that of the surrounding particles (phase 2), and the jump of pressure between the two phases satisfy the condition

$$\Delta \mathrm{p} = \frac{\beta}{R} = \frac{\beta\sqrt{\pi}}{L_a} \tag{63}$$

where R denotes the equilibrium radius of drop. Fig.12 shows the cut of the pressure field at Y=0.1(X-axis) obtained in the simulations and also the analytical pressure predicted by Laplace's law.

And the pressure coefficient C_p is calculated as

$$C_p = \frac{\left|p_{phase1} - p_{phase2}\right|}{\Delta p} \tag{64}$$

As the number of particles increase, numerical results are gradually consistent with the theoretical pressure. When $l_s/200$, it is observed a good agreement between the numerical results and the

theoretical pressure. These results show that the AC-CSF model is able to represent correctly the equilibrium state of this two-phase flow problem. Note that, pressure profile with Interface-PSA in Fig. 13 is lower than that without Interface-PSA. And it is also found that the impact on pressure is slight.

To further testify the present model, the deformation of cubic liquid drop is simulated, which will finally evolve a sphere. The initial condition, including initial density, side length, viscosity, and surface tension coefficient is totally the same as the 2D liquid drop. Fig. 14 shows the snapshot of shape, pressure, and velocity field of cubic liquid drop for particle resolution $l_s/50$. Due to surface tension force on the surface of a cubic liquid drop, the eight corners of the cubic liquid drop deform first. During the oscillation, cubic liquid drop evolves into a dumbbell, diamond, sphere at equilibrium.

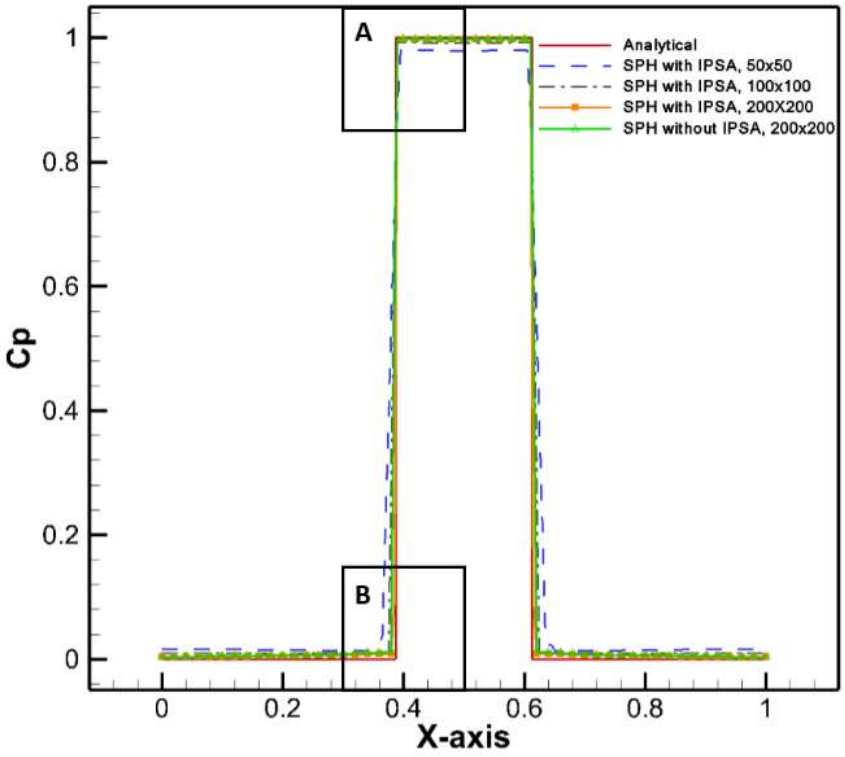

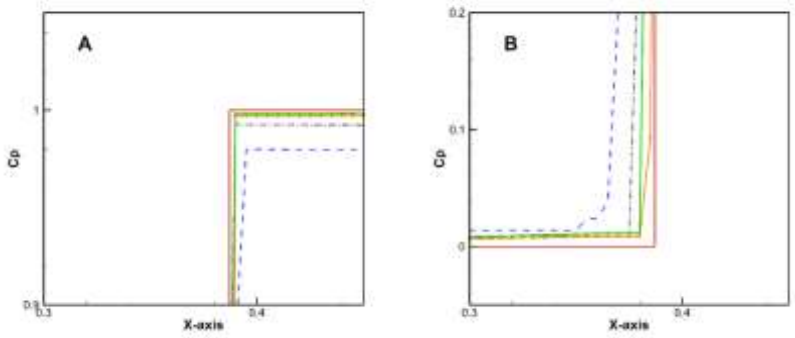

Fig.11. The cut of the pressure field at Y=0.1(X-axis).

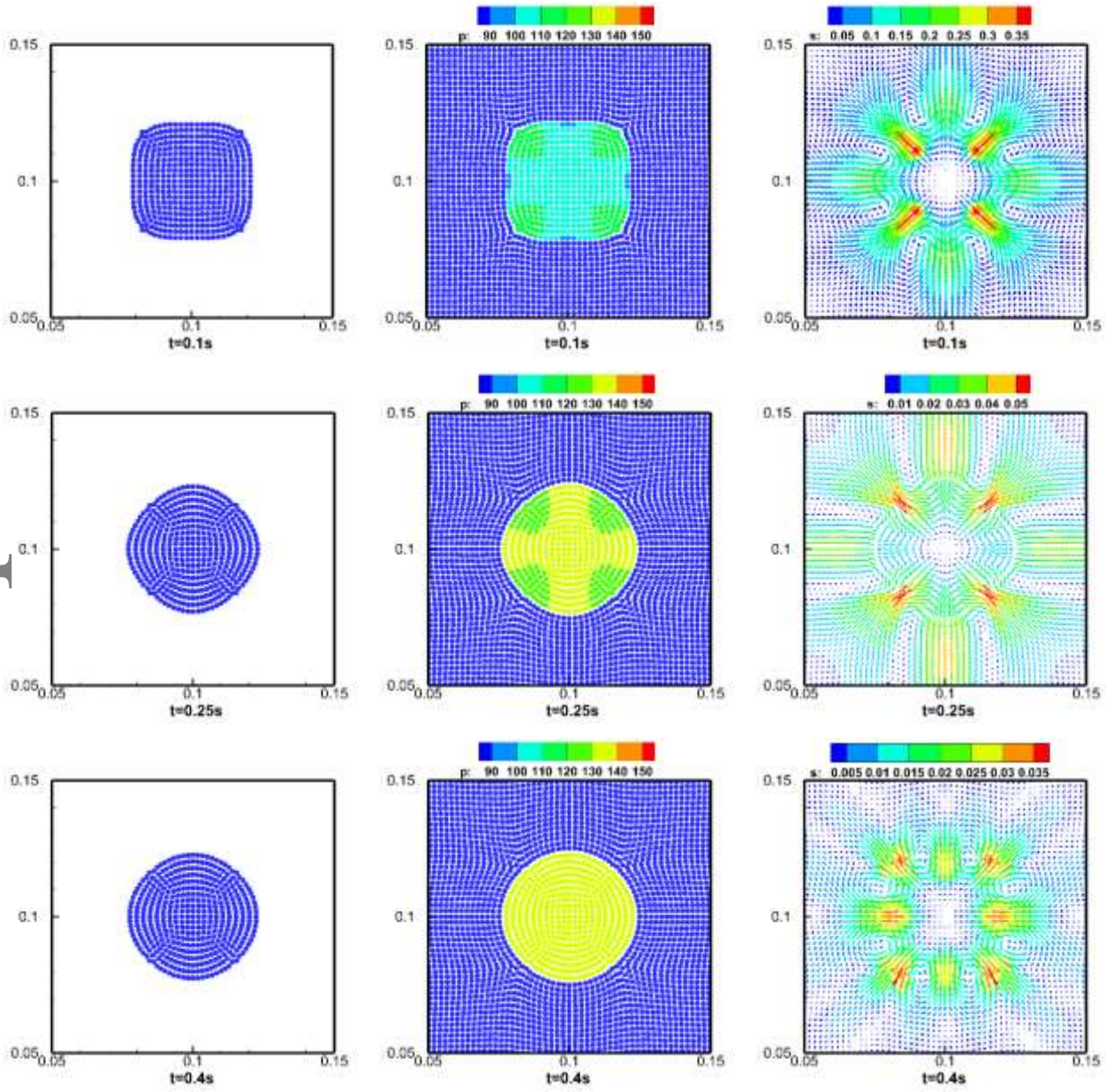

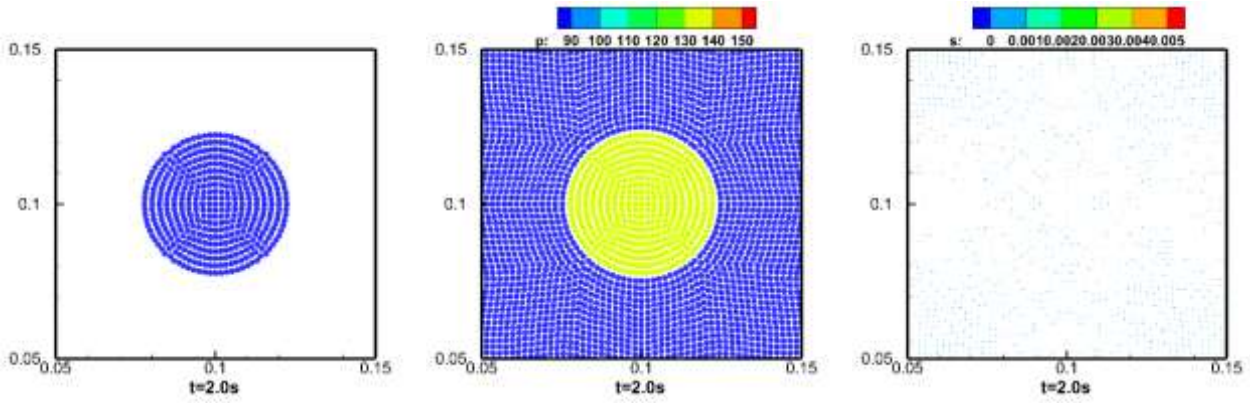

Fig. 12. The snapshots of shape evolution, the pressure field and velocity magnitude for 2D square droplet.

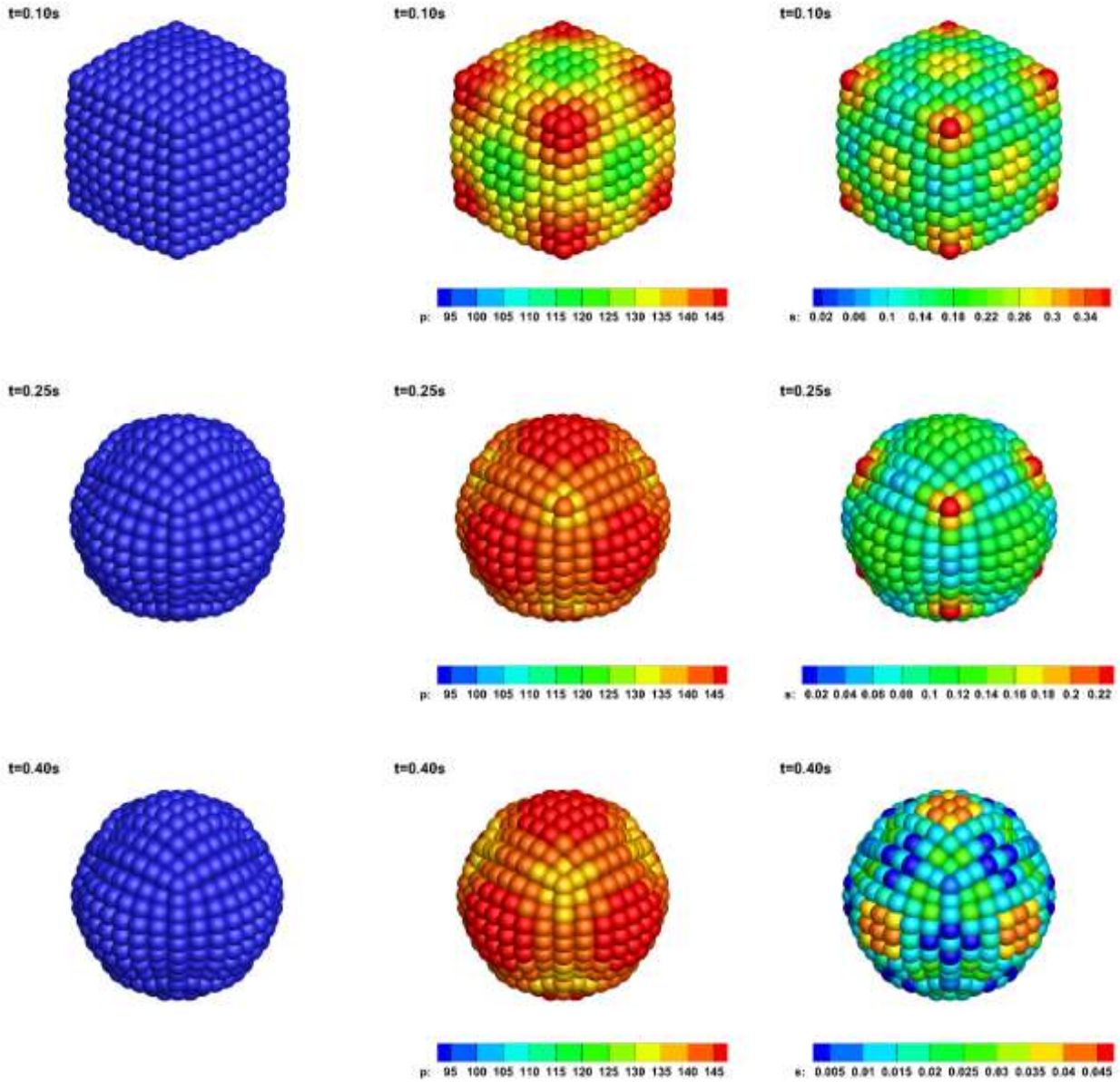

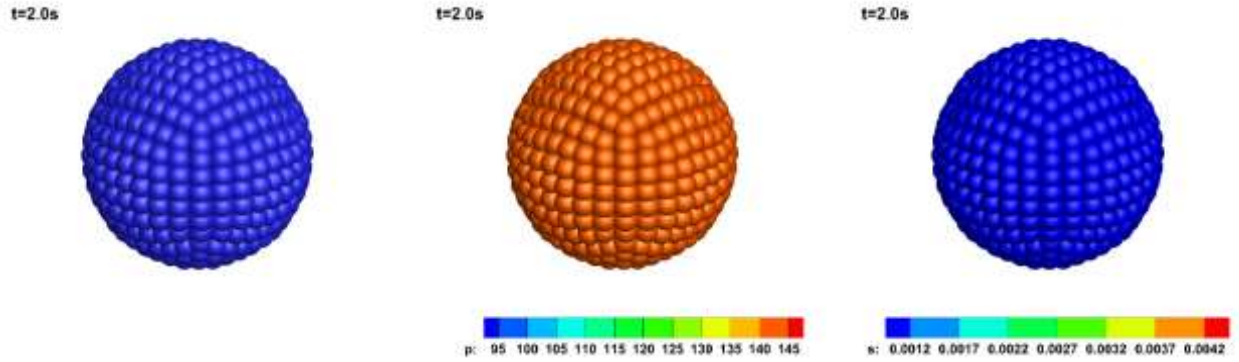

Fig. 13. The snapshots of shape evolution, the pressure field and velocity magnitude for 3D cubic droplet.

4.3 Rayleigh-Taylor instability

As a benchmark configuration, the Rayleigh-Taylor instability problem is considered, which was also studied by some other researchers, including Cummins and Rudman [54]; Grenier et al. [13]; Chen et al. [15]. The very complex interface obtained is not easy for numerical modeling. In this problem, the computation is performed in a rectangle container ($L_x \times L_y = 1\ \mathrm{m} \times 2\ \mathrm{m}$) with a heavier fluid placed Ω_1 on a lighter fluid Ω_2, as shown in Fig.14 (e.g. the density ratio of heavier fluid and the lighter fluid is 1.8). The two fluids are separated by an interface perturbed according to $y_x = 1.0 - 0.15\,sin(2\pi x)$. The Reynolds number is $Re = \sqrt{(L_y/2)^3 g}/\nu = 420$ based on an equal kinematic viscosity ν for both fluids. The gravity acceleration is $g = 1.0\ \mathrm{m/s^2}$.

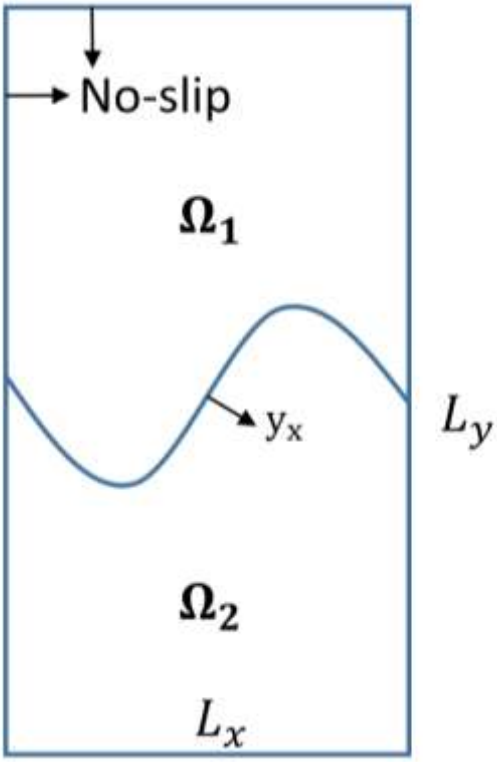

Fig.14. Illustration of initial Rayleigh-Taylor instability model.

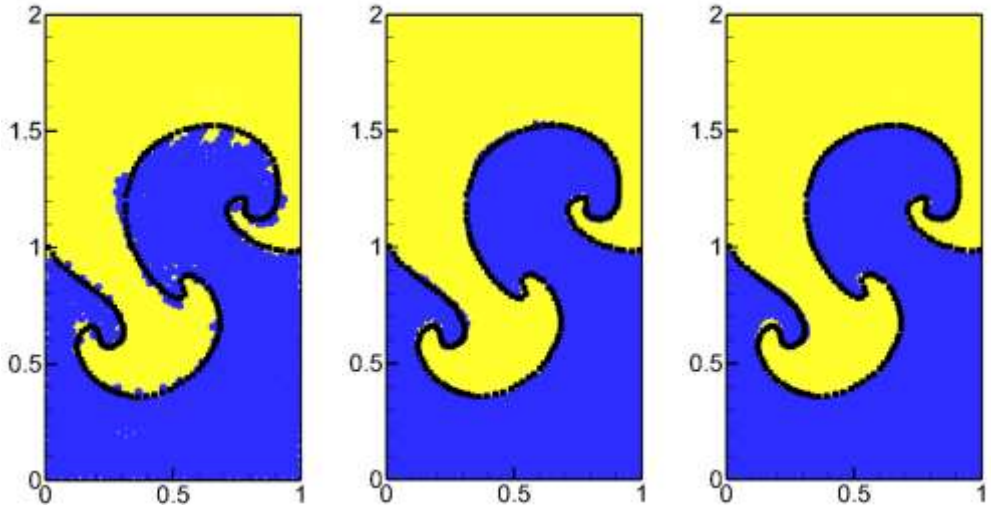

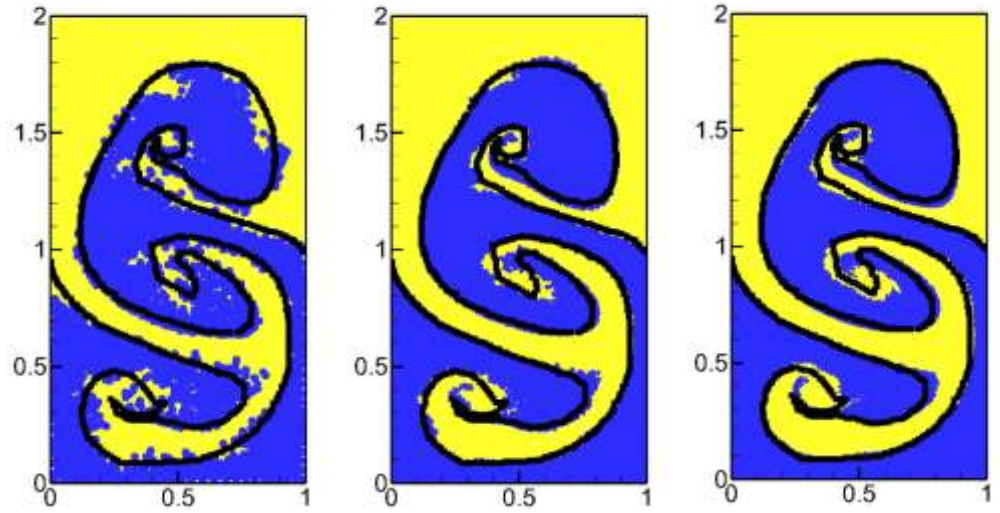

Fig.15. Snapshots of Interface shape with different particle resolutions (Blackline is Level set results [55]) $(50 \times 100, 100 \times 200, 200 \times 400)$ from left to right (At two different times t = 3 s (up), t = 5 s (down)).

The particles have an initial regular lattice distribution. In Fig.15 we compare three different particle resolutions $(50 \times 100, 100 \times 200, 200 \times 400)$ at two different times t = 3 s, t = 5 s. Quantitatively, it's shown that the three-particle resolutions are able to simulate substantially the same phenomena of the Rayleigh-Taylor instability problem. Nevertheless, at the low resolution 50 × 100, the roll-up of the small structures at the mushroom-shaped head is not well reproduced. For the finer resolutions, all the small structure phenomena due to the development and roll-up of the mushroom-shaped heads are captured at t = 3s. The two finer resolutions (99 ×199 and 150 ×300) are very similar to each other in terms of the shape of the instability, comparing well with the results of the Level set [55]. However, there are also some differences near the plumes, which is a larger formation of the roll-up, due to different numerical methods.

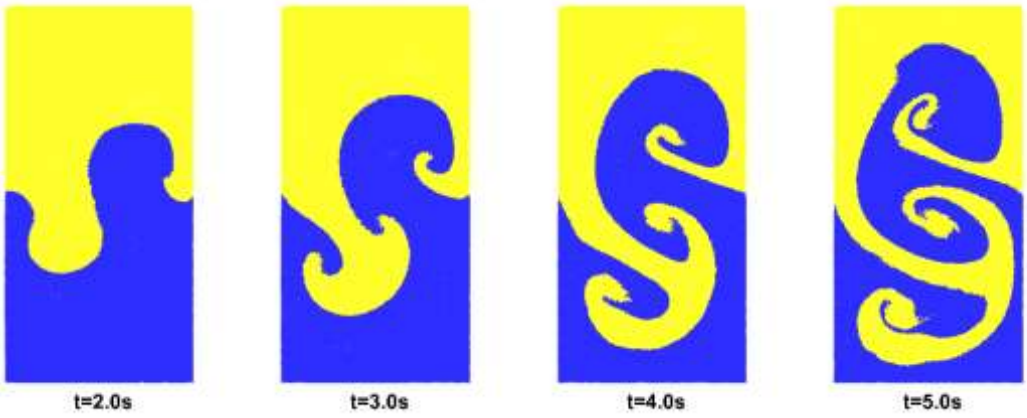

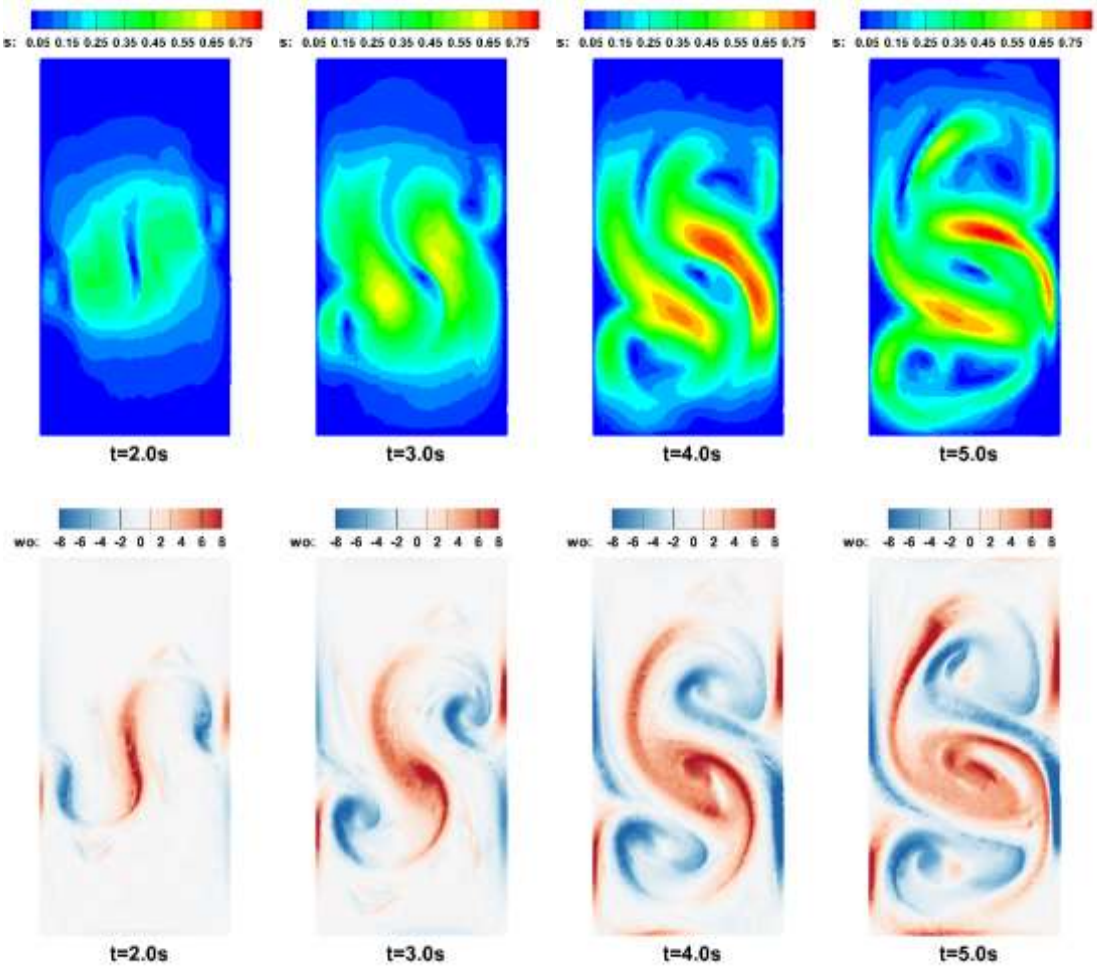

Fig.16.The phase distribution, velocity magnitude and the vorticity top to bottom for particle resolution 200×400.

Fig.16 depicts the phase distribution, velocity field and the vorticity for four consecutive times at $t = 2$ s, $t = 3$ s, $t = 4$ s, $t = 5$ s. It is seen that the density difference between the heavy and light fluids leads to instability, and this two-fluid system starts to evolve due to gravity and generates complex fluid interface. The initial distortion entails vorticity generation at the interface. In close proximity to the interface, phase 2 has a larger velocity gradient in interface normal direction and due to incompressibility, the velocity gradient in interface tangential direction is larger as well. This leads to broader plumes of phase 2. Due to the central vortex, the plumes are deflected counterclockwise. The highest point of phase 1 fluid for the three-particle resolutions ($50 \times 100, 100 \times 200, 200 \times 400$) is plotted in Fig.17 together with the curve obtained using Layzer's theory [56]. The results are in good agreement with the Layzer theory. Meanwhile, Interface–PSA has some slight influence on the results, which is a similar conclusion as in the Dam breaking case.

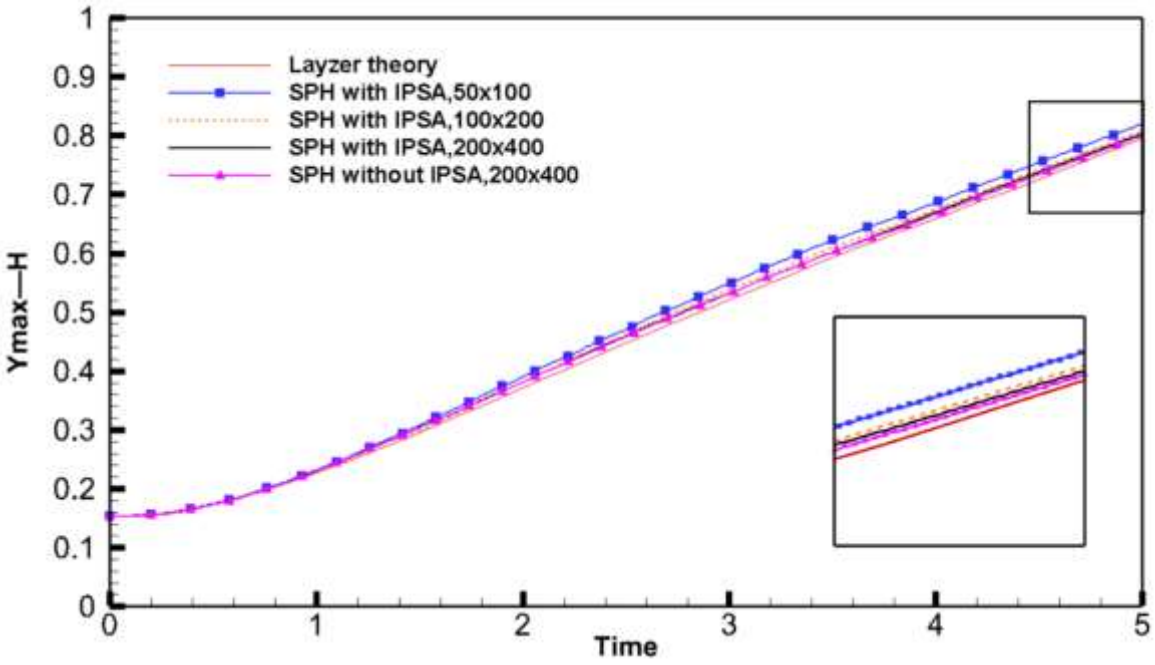

Fig. 17. The time variation of the highest point of phase 1 fluid.

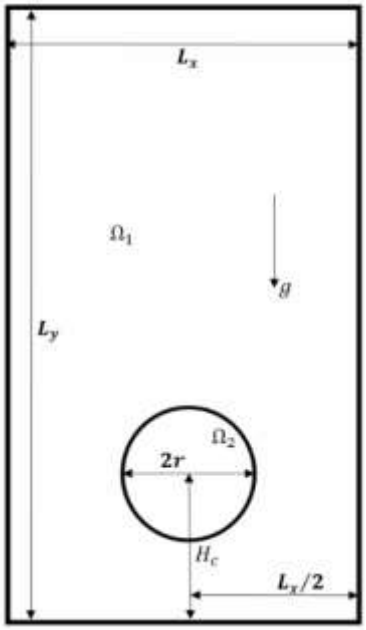

Fig.18. Illustration of initial bubble rising.

4.4 Bubble rising

In this section, the newly proposed two-phase SPH model is further tested and validated against the published results related to bubble rising in viscous fluids, which are strongly affected by fluid viscosity and surface tension. For large scare bubble rising problems, surface tension has less influence. In previous work, it's found that there is unphysical infiltration over the interface. Interface repulsive has been introduced by [5, 13, 22, 47, 57-59] to simulate bubbles rising. Here, an interface force is added in the acceleration as following

$$F_I = -\epsilon \frac{1}{m_i} \sum_{\mathfrak{D}} \left(\frac{V_i^2 P_i}{\Gamma_i} + \frac{V_j^2 P_j}{\Gamma_j} \right) \nabla_i W_{ij} \tag{65}$$

where $\epsilon = 0.08$ is the interface force coefficient, and the label $\mathfrak{D}$ denotes summation applies to neighbor particles j in the phase different from particles i. For case 1, this case involves the rising of an air bubble in water, which was also modeled by Sussman et al. [60] using the Level-Set algorithm to track the fluid interface. In fact, this case has been tested in many works [57]. In this example, the radius of the bubble is $R = 0.1$ m. The width L_x and height L_y of the tank are $6R$ and $10R$, as shown in Fig.18. The problem involves a density ratio of 1000 (water density 1000 kg/m^3 and air density 1.0 kg/m^3) and a dynamics viscosity are water density 0.035 Pa. s and air density 0.0065 Pa. s. The initial time stepping is 2.5×10^{-6} s. The initial particle space is 0.0025 m and with a total number of 480,000 particles (240×400 along x and y direction). The interface tension coefficient is $\sigma = 0.126\,\mathrm{N/m}$. The gravity acceleration is $g = 9.81\,\mathrm{m/s^2}$. A positive background pressure is taken as $p_b = 1200$ Pa.

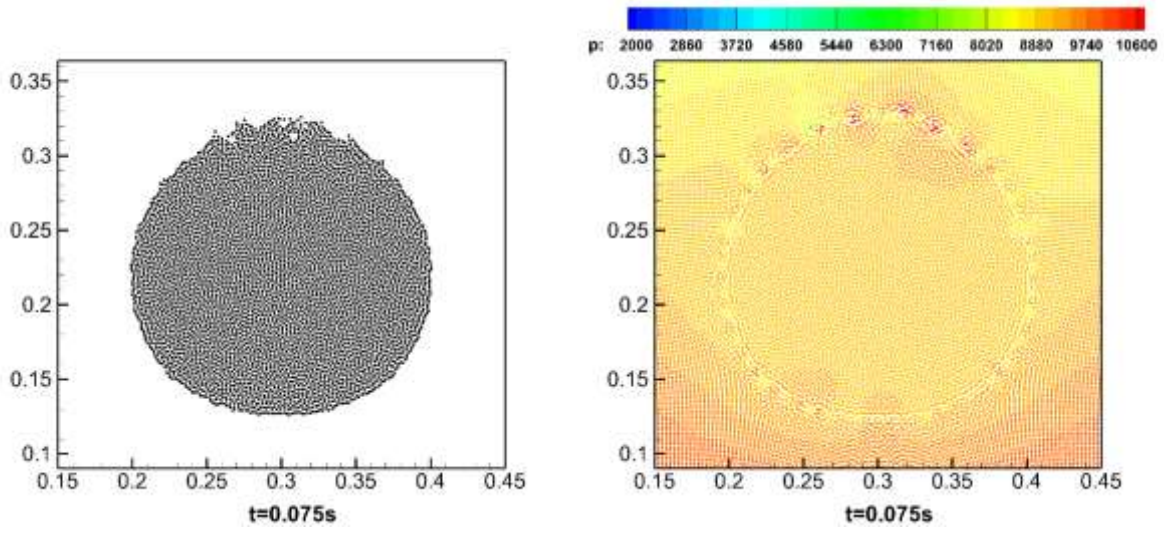

Fig.19. Bubble shape and pressure field of bubble rising case with original PSA at 0.075s.

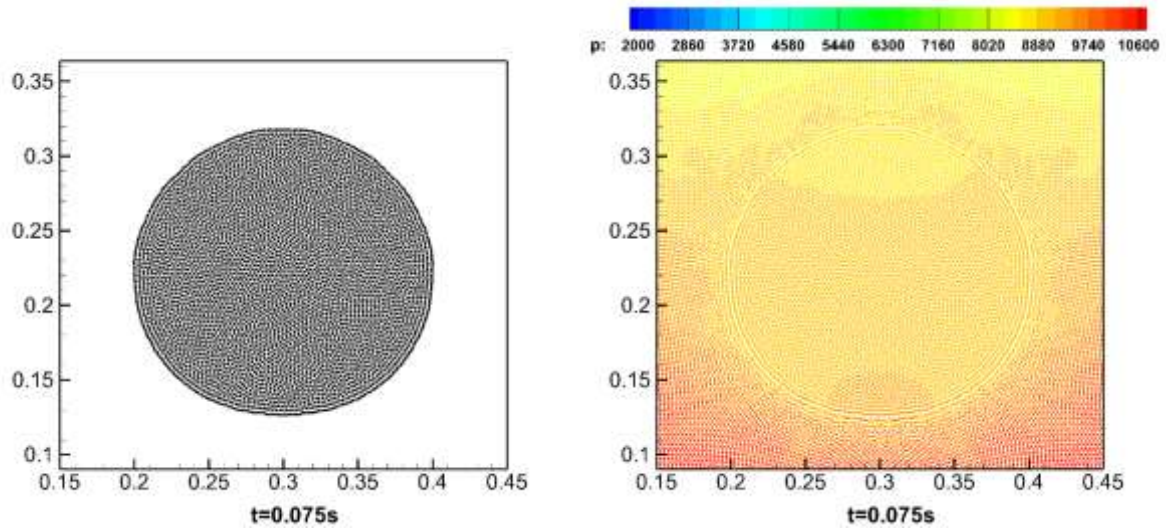

Fig.20. Bubble shape and pressure field of bubble rising case with interface-PSA at 0.075s.

Fig.19 shows the phase distribution and pressure field of bubble rising with traditional PSA at $t = 0.07$s. It is obviously that some gas particles unphysically penetrate into water flows, and this leads to a nonphysical rough interface. Meanwhile, the pressure field near the interface is no longer smooth. Fig.20 shows the phase distribution and pressure field of bubble rising with interface-PSA at $t = 0.07$s. It's shown that Interface-PSA is proved to maintain interface stability for interfacial flow problems.

Fig.21 shows the pressure field (left half) and bubble shape (right half) at 9 sequencing instants as it raises in water (water particles are not plotted). It is seen that the present SPH model can well capture the water-air interface. As time passes, the upwelling water motion deforms the bubble, which attains a horseshoe shape. After that, the extremities roll-up until they undergo a big deformation which subsequently splits the bubble to form other small ones. The main difference between the results is that near to the symmetric axis, the bubble obtained using the present SPH method is thicker than the one obtained by the level-Set method. The results for the width of the bubble remains in very good agreement during all the simulation period for both methods. We observe that in the Level-set solution, the bubble splits in several very small bubbles that are not predicted by the present SPH method. For example, before $t\sqrt{g/h} = 4.4$ while the bubble nearly pinches off, the thickness of the bubble from present SPH simulation is slightly smaller than that in Level-Set simulation. At $t\sqrt{g/h} = 4.8$, and the Level-Set simulation predicts four bubbles (two larger bubbles and two smaller next to the two major bubbles). Thereafter, these smaller bubbles disappear gradually from the Level-Set simulation. The bubble rising problem was also investigated

by other people using the SPH method [5, 17] and they found the same discrepancies between SPH and Level-Set results[60].

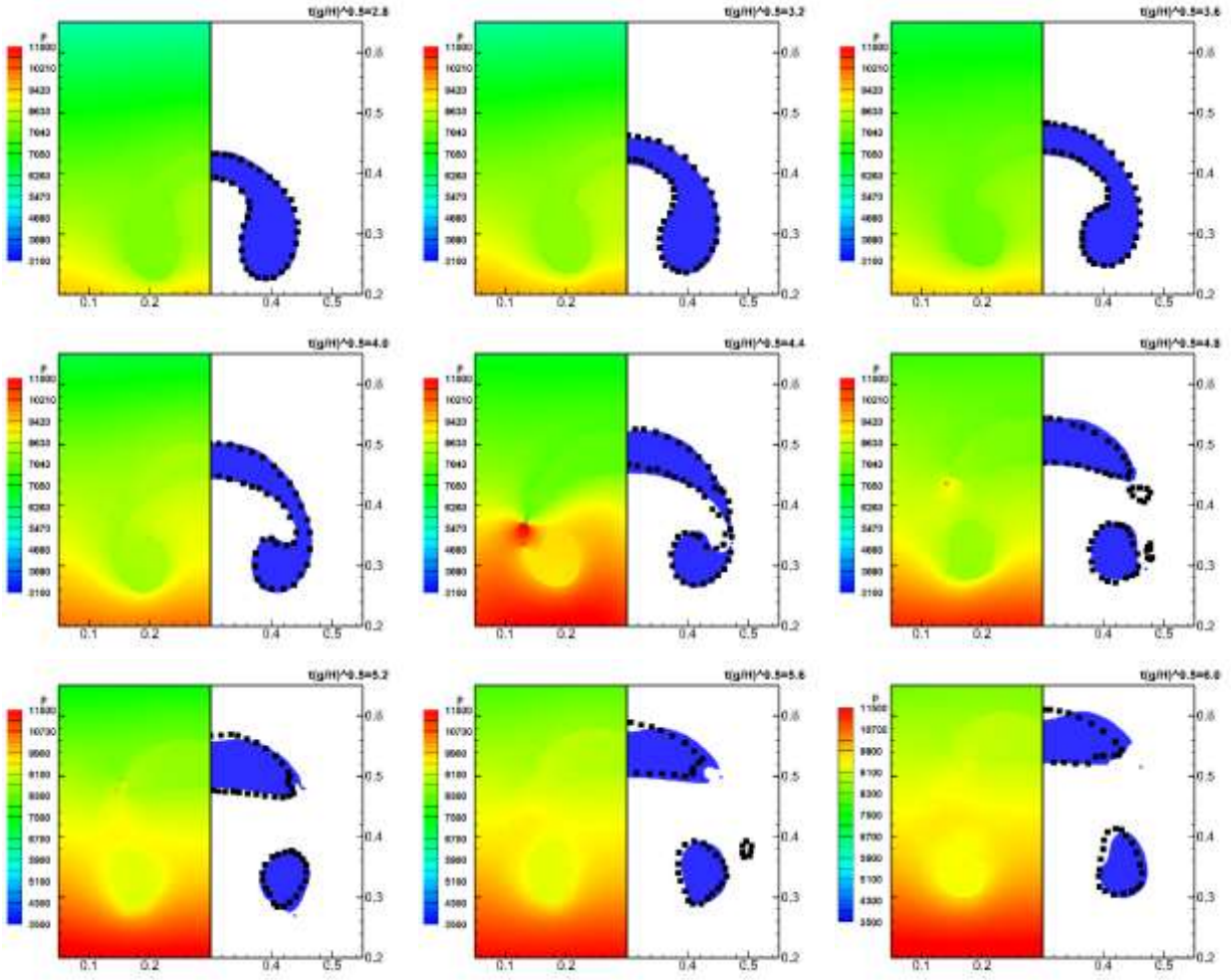

Fig.21. Pressure field (left half) and bubble shape (right half) at nine-time instances. The water-air interface (marked by black dots) obtained from Level-Set simulation [60].

For case 2, based on the definition in Hysing et al. [61], a two-dimensional computational domain with $L_x/L_y = 4R/8R$ is adopted with the free-slip condition being imposed at left and right walls and non-slip boundary at the top and bottom walls. A bubble with the radius of $R = 0.25$ m is initially set at $(L_x/2\,, H_c) = (2R, 2R)$. Assigned to fluids inside and outside the bubble are $\rho_{\Omega_2} = 100\,\mathrm{kg/m^3}$ and $\rho_{\Omega_1} = 1000\,\mathrm{kg/m^3}$, respectively. The viscosities are $\mu_{\Omega_2} = 1$ Pa s and $\mu_{\Omega_1} = 10$ Pa s and the interface tension coefficient is $\sigma = 24.5\,\mathrm{N/m}$. The gravity acceleration is $g = 0.98\,\mathrm{m/s^2}$. A positive background pressure is taken as $p_b = 800$ Pa.

During bubble rising and shape translation, the centroid position of the bubble Y_C and velocity U_C, may be used to track the bubble movement and are determined as[22]

$$\begin{cases} Y_C = \dfrac{\sum_i^{N_{\Omega_2}} y_i}{N_{\Omega_2}} \\ U_C = \dfrac{\sum_i^{N_{\Omega_2}} u_i^y}{N_{\Omega_2}} \end{cases} \tag{66}$$

where y_i and u_i^y is the vertical coordinate and velocity of the bubble particle i. The time evolution of the center of mass and rising velocity, as shown in Fig.22, where the SPH results of all the two-particle resolutions (i.e., 50×100 and 100×200) agree well with the reference data. Though there are some oscillations observed for rising velocity, the overall trend is in accordance with the reference data. The bubble shape and pressure distribution with the particle number of 100×200 at t=1 s, t = 2 s, t = 3 s are shown in Fig.23, showing very good agreement with the reference results. The pressure field is smooth and the interface is sharp and stable.

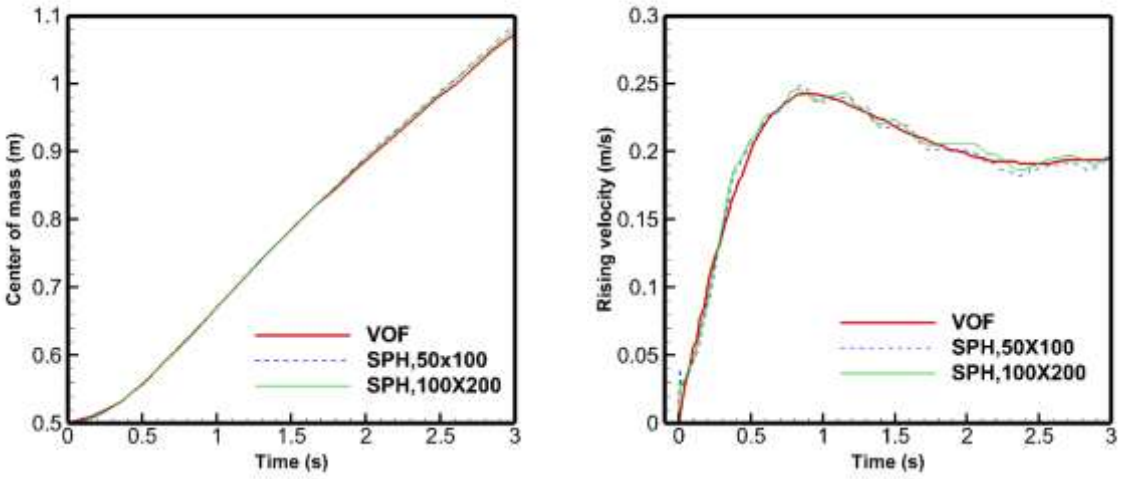

Fig.22.The time evolution of the center of mass (left) and the rising velocity (right).

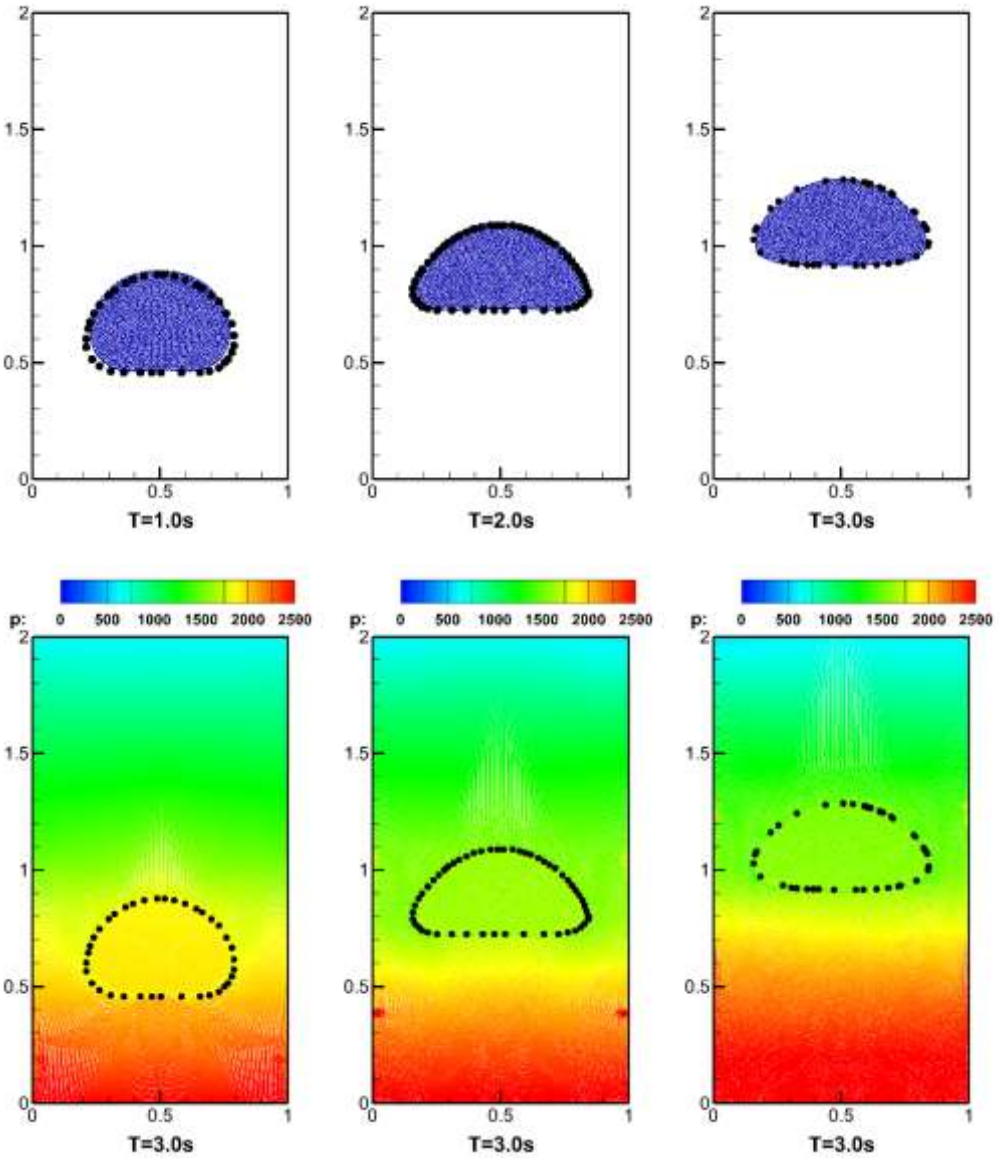

Fig.23.The shape and pressure field for the rising bubble compared with the results from Hysing et al. [61] (marked by black dots).

5 Conclusion

This paper presents a SPH model for complex interfacial flows with large density ratios. The discrete continuity equation is obtained by considering the time derivative of the volume of the particle. The Eckart's continuum Lagrange is introduced here to derive the discrete acceleration equation. Only the particle volume and position make a contribution to neighboring particles.

A continuum surface force (CSF) model is used to meet the realistic configurations. The pressure difference between the in-outside of the droplet agreeing well with Laplace law and the convergent result declares that the CSF model is accurate and robust. And the similar the gradient of

the color function with the formulation proposed by Adami et al. [23] suggests their model also meets the assumption of acceleration continuity. An improved boundary condition is presented to simulate free-slip and no-slip wall conditions for interfacial flow problems. The stable interface near the wall and precise pressure prediction in dam breaking case indicate that boundary condition in this work is suitable and robust for interfacial flows with big density ratios. Then particle shifting algorithm (PSA) is improved for interfacial flows by imposing the normal correction near the interface. In dam-breaking cases, compared to the results without Interface-PSA, the pressure curve indicates Interface-PSA can reduce pressure oscillation and numerical noise. While Interface-PSA has a slight influence on interface position and shape in other validation cases, which results from limited position correction near the interface. In bubble rising cases, present interface-PSA can maintain the smooth bubble interface compared to the original PSA.

All four numerical examples are investigated and compared with analytic solutions and widely accepted numerical results and experimental data. It is demonstrated that the present integrated SPH model can well capture interfacial flow physics with various viscosity and big density ratios, surface tension and the dynamic evolution of the complex interfaces.

Acknowledgment

The present work is supported by, Qingdao National Laboratory for Marine Science and Technology (QNLM2016ORP0402) , the National Natural Science Foundation of China (51522902, 51579040) ,the Fundamental Research Funds for the Central Universities（DUT17ZD233）,the No. [2016] 22 supported by Ministry of Industry and Information Technology of China. The first author gratefully acknowledges the financial support from the China Scholarship Council (Grant No. 201806060137). The authors would also like to thank the anonymous reviewers for the fruitful suggestions.

Reference

[1] M. B. Liu and G. R. Liu. "Smoothed Particle Hydrodynamics (SPH): an Overview and Recent Developments," *Archives of Computational Methods in Engineering* 2010;17(1): 25-76.

[2] T. Ye, D. Pan, C. Huang, and M. Liu. "Smoothed particle hydrodynamics (SPH) for complex fluid flows: Recent developments in methodology and applications," *Physics of Fluids 2019;* 31(1): 011301.

[3] A. M. Tartakovsky, N. Trask, K. Pan, B. Jones, W. Pan, and J. R. Williams. "Smoothed particle hydrodynamics and its applications for multiphase flow and reactive transport in porous media," *Computational Geosciences 2016;* 20(4): 807-834.

[4] J. J. Monaghan and A. Kocharyan. "SPH simulation of multi-phase flow," *Computer Physics Communications 1995;* 87(1): 225-235.

[5] A. Colagrossi and M. Landrini. "Numerical simulation of interfacial flows by smoothed particle hydrodynamics," *Journal of Computational Physics 2003;* 191(2): 448-475.

[6] X. Yang and S.-C. Kong. "Adaptive resolution for multiphase smoothed particle hydrodynamics," *Computer Physics Communications* 2019.

[7] A. Rahmat and M. Yildiz. "A multiphase ISPH method for simulation of droplet coalescence and electro-coalescence," *International Journal of Multiphase Flow 2018;* 105: 32-44.

[8] F. R. Ming, P. N. Sun, and A. M. Zhang. "Numerical investigation of rising bubbles bursting at a free surface through a multiphase SPH model," *Meccanica 2017*;52(11): 2665-2684.

[9] A. Zainali, N. Tofighi, M. S. Shadloo, and M. Yildiz. "Numerical investigation of Newtonian and non-Newtonian multiphase flows using ISPH method," *Computer Methods in Applied Mechanics and Engineering 2013;* 254: 99-113.

[10] M. Liu and Z. Zhang, "Smoothed particle hydrodynamics (SPH) for modeling fluid-structure interactions," *Science China Physics, Mechanics & Astronomy 2019,* 62(8): 984701.

[11] X. Y. Hu and N. A. Adams. "A multi-phase SPH method for macroscopic and mesoscopic flows," *Journal of Computational Physics 2006;* 213(2): 844-861.

[12] X. Y. Hu and N. A. Adams. "An incompressible multi-phase SPH method," *Journal of Computational Physics 2007;* 227(1): 264-278.

[13] N. Grenier, M. Antuono, A. Colagrossi, D. Le Touzé, and B. Alessandrini. "An Hamiltonian interface SPH formulation for multi-fluid and free surface flows," *Journal of Computational Physics 2009;* 228(22): 8380-8393.

[14] J. J. Monaghan and A. Rafiee. "A simple SPH algorithm for multi-fluid flow with high density ratios," *International Journal for Numerical Methods in Fluids 2012;* 71(5): 537-561.

[15] Z. Chen, Z. Zong, M. B. Liu, L. Zou, H. T. Li, and C. Shu. "An SPH model for multiphase flows with complex interfaces and large density differences," *Journal of Computational Physics 2015*; 283: 169-188.

[16] S. J. Lind, P. K. Stansby, and B. D. Rogers. "Incompressible–compressible flows with a transient discontinuous interface using smoothed particle hydrodynamics (SPH)," *Journal of Computational Physics 2016;* 309: 129-147.

[17] A. Krimi, M. Rezoug, S. Khelladi, X. Nogueira, M. Deligant, and L. Ramírez. "Smoothed Particle Hydrodynamics: A consistent model for interfacial multiphase fluid flow simulations," *Journal of Computational Physics 2018;* 358: 53-87.

[18] C. Eckart, "VARIATION PRINCIPLES OF HYDRODYNAMICS," *Physics of Fluids 1960;* 3(3): 421-427.

[19] V. Springel and L. Hernquist. "Cosmological smoothed particle hydrodynamics simulations: the entropy equation," *Monthly Notices of the Royal Astronomical Society 2002;* 333(3): 649-664.

[20] J. U. Brackbill, D. B. Kothe, and C. Zemach. "A continuum method for modelling surface tension,"

Journal of Computational Physics 1992; 100(2): 335-354.

[21] J. P. Morris. "Simulating surface tension with smoothed particle hydrodynamics," *International Journal for Numerical Methods in Fluids 2000;* 33(3): 333-353.

[22] A. Zhang, P. Sun, and F. Ming. "An SPH modelling of bubble rising and coalescing in three dimensions," *Computer Methods in Applied Mechanics and Engineering 2015;* 294: 189-209.

[23] T. Breinlinger, P. Polfer, A. Hashibon, and T. Kraft. "Surface tension and wetting effects with smoothed particle hydrodynamics," *Journal of Computational Physics 2013;* 243: 14-27.

[24] M. Zhang, "Simulation of surface tension in 2D and 3D with smoothed particle hydrodynamics method," *Journal of Computational Physics 2010,* 229 (19): 7238-7259.

[25] X. Yang, M. Liu, and S. Peng, "Smoothed particle hydrodynamics modeling of viscous liquid drop without tensile instability," *Computers & Fluids 2014,* 92: 199-208.

[26] S. Adami, X. Y. Hu, and N. A. Adams. "A new surface-tension formulation for multi-phase SPH using a reproducing divergence approximation," *Journal of Computational Physics 2010;* 229(13): 5011-5021.

[27] R. Xu, P. Stansby, and D. Laurence. "Accuracy and stability in incompressible SPH (ISPH) based on the projection method and a new approach," *Journal of Computational Physics 2009;*228(18): 6703-6725.

[28] S. J. Lind, R. Xu, P. K. Stansby, and B. D. Rogers. "Incompressible smoothed particle hydrodynamics for free-surface flows: A generalised diffusion-based algorithm for stability and validations for impulsive flows and propagating waves," *Journal of Computational Physics 2012;* 231(4): 1499-1523.

[29] A. Khayyer, H. Gotoh, and Y. Shimizu. "Comparative study on accuracy and conservation properties of two particle regularization schemes and proposal of an optimized particle shifting scheme in ISPH context," *Journal of Computational Physics 2017;*332: 236-256.

[30] P. N. Sun, A. Colagrossi, S. Marrone, and A. M. Zhang. "The δplus-SPH model: Simple procedures for a further improvement of the SPH scheme," *Computer Methods in Applied Mechanics and Engineering* 2017; 315: 25-49.

[31] A. Skillen, S. Lind, P. K. Stansby, and B. D. Rogers. "Incompressible smoothed particle hydrodynamics (SPH) with reduced temporal noise and generalised Fickian smoothing applied to body–water slam and efficient wave–body interaction," *Computer Methods in Applied Mechanics and Engineering 2013;* 265: 163-173.

[32] A. Mokos, B. D. Rogers, and P. K. Stansby. "A multi-phase particle shifting algorithm for SPH simulations of violent hydrodynamics with a large number of particles," *Journal of Hydraulic Research 2017;* 55(2): 143-162.

[33] J. P. Morris, P. J. Fox, and Y. Zhu. "Modelling Low Reynolds Number Incompressible Flows Using SPH," *Journal of Computational Physics 1997;* 136(1): 214-226.

[34] J. J. Monaghan. "Simulating Free Surface Flows with SPH," *Journal of Computational Physics 1994;* 110(2): 399-406.

[35] S. Marrone, A. Colagrossi, M. Antuono, G. Colicchio, and G. Graziani. "An accurate SPH modelling of viscous flows around bodies at low and moderate Reynolds numbers," *Journal of Computational Physics 2013*; 245: 456-475.

[36] A. Colagrossi, B. Bouscasse, M. Antuono, and S. Marrone. "Particle packing algorithm for SPH schemes," *Computer Physics Communications 2012;* 183(8): 1641-1653.

[37] S. Koshizuka, A. Nobe, and Y. Oka. "Numerical analysis of breaking waves using the moving particle semi-implicit method," *International Journal for Numerical Methods in Fluids 1998;* 26(7): 751-769.

[38] T. Belytschko, Y. Krongauz, J. Dolbow, and C. Gerlach, "On the completeness of meshfree particle methods," *International Journal for Numerical Methods in Engineering 1998;* 43(5): 785-819.

[39] G. Oger, M. Doring, B. Alessandrini, and P. Ferrant, "An improved SPH method: Towards higher order convergence," *Journal of Computational Physics 2007,* 225(2): 1472-1492.

[40] G. Duan, S. Koshizuka, A. Yamaji, B. Chen, X. Li, and T. Tamai, "An accurate and stable multiphase moving particle semi‐implicit method based on a corrective matrix for all particle interaction models," *International Journal for Numerical Methods in Engineering 2018,* 115(10): 1287-1314.

[41] C. Eckart, "Variation Principles of Hydrodynamics," *The Physics of Fluids 1960;* 3(3): 421-427.

[42] J. J. Monaghan and R. A. Gingold. "Shock simulation by the particle method SPH," *Journal of Computational Physics 1983;* 52(2): 374-389.

[43] S. Adami, X. Y. Hu, and N. A. Adams. "A generalized wall boundary condition for smoothed particle hydrodynamics," *Journal of Computational Physics 2012;* 231(21): 7057-7075.

[44] A. M. Xenakis, S. J. Lind, P. K. Stansby, and B. D. Rogers. "An incompressible SPH scheme with improved pressure predictions for free-surface generalised Newtonian flows," *Journal of Non-Newtonian Fluid Mechanics 2015;* 218: 1-15.

[45] Y. Zhu and P. J. Fox. "Smoothed Particle Hydrodynamics Model for Diffusion through Porous Media," *Transport in Porous Media 2001;* 43(3): 441-471.

[46] J. J. Monaghan. "Smoothed particle hydrodynamics," *Reports on Progress in Physics 2005;* 68(8): 1703.

[47] G. X. Zhu, L. Zou, Z. Chen, A. M. Wang, and M. B. Liu. "An improved SPH model for multiphase flows with large density ratios," *International Journal for Numerical Methods in Fluids 2018;* 86(2): 167-184.

[48] S. Marrone, M. Antuono, A. Colagrossi, G. Colicchio, D. Le Touzé, and G. Graziani. "δ-SPH model for simulating violent impact flows," *Computer Methods in Applied Mechanics and Engineering 2011;* 200(13): 1526-1542.

[49] M. Greco, M. Landrini, and O. M. Faltinsen. "Impact flows and loads on ship-deck structures," *Journal of Fluids and Structures 2004;* 19(3): 251-275.

[50] Z. Q. Zhou, J. O. D. Kat, and B. Buchner. "A nonlinear 3D approach to simulate green water dynamics on deck," in *Seventh international conference on numerical ship hydrodynamics* 1999, 1-4.

[51] M. Hirschler, G. Oger, U. Nieken, and D. Le Touzé. "Modelling of droplet collisions using Smoothed Particle Hydrodynamics," *International Journal of Multiphase Flow 2017;* 95: 175-187.

[52] E. Shigorina, J. Kordilla, and A. M. Tartakovsky. "Smoothed particle hydrodynamics study of the roughness effect on contact angle and droplet flow," *Physical Review E 2017;* 96(3): 033115.

[53] M. Zhang and X.-L. Deng. "A sharp interface method for SPH," *Journal of Computational Physics 2015;* 302: 469-484.

[54] S. J. Cummins and M. Rudman. "An SPH Projection Method," *Journal of Computational Physics 1999;* 152(2): 584-607.

[55] G. Colicchio, "Violent disturbance and fragmentation of free surfaces," Ph.D Thesis, University of Southampton, 2005.

[56] D. Layzer. "On the instability of superposed fluids in a gravitational field," *The astrophysical journal 1955;*122: 1.

[57] L. Zou, G. X. Zhu, Z. Chen, Y. G. Pei, and Z. Zong. "Numerical Investigation on the Water Entry of Convex Objects Using a Multiphase Smoothed Particle Hydrodynamics Model," *International Journal of Computational Methods 2017;* 15(02): 1850008.

[58] X. Liu, R. Ogawa, M. Kato, K. Morita, and S. Zhang, "Accuracy and stability enhancements in the incompressible finite-volume-particle method for multiphase flow simulations," *Computer Physics Communications 2018,* 230: 59-69.

[59] X. Liu, Y. Aramaki, L. Guo, and K. Morita, "Numerical simulation of gas–liquid–solid three-phase flow using particle methods," *Journal of Nuclear Science and Technology 2015,* 52(12): 1480-1489.

[60] M. Sussman, P. Smereka, and S. Osher. "A Level Set Approach for Computing Solutions to Incompressible Two-Phase Flow," *Journal of Computational Physics 1994;* 114(1): 146-159.

[61] S. Hysing. "Quantitative benchmark computations of two-dimensional bubble dynamics," *International Journal for Numerical Methods in Fluids. 2008;* 60(11): 1259-1288.

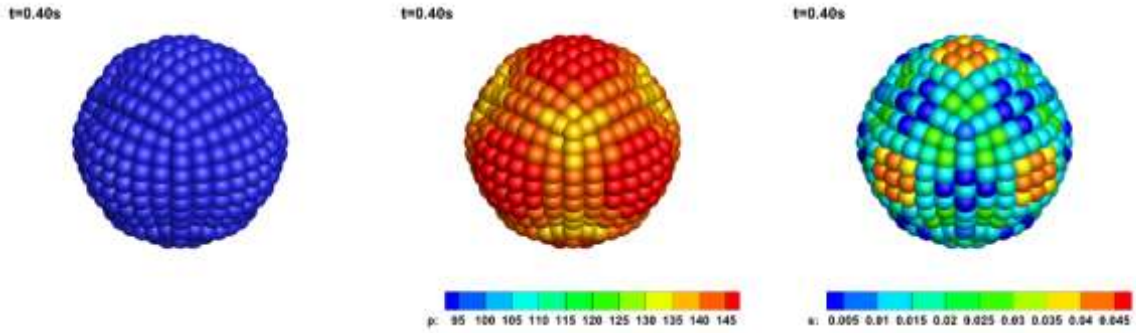

Title: An Integrated Smoothed Particle Hydrodynamics Model for Complex Interfacial Flows with Large Density Ratios

Author: G.X. Zhu, L. Zou*

***Mini-abstract**:* An integrated smoothed particle hydrodynamics (SPH) model for complex interfacial flows with large density ratios is developed. The discrete continuity equation and acceleration equation are obtained by considering the time derivative of the volume of particle and Eckart's continuum Lagrangian equation. Interface-PSA is added for interfacial flows by imposing the normal correction near the interface.